Computer Modeling in Engineering & Sciences

Tech Science Press

DOI: 10.32604/cmes.2022.021676

ARTICLE

Analysis and Power Quality Improvement in Hybrid Distributed Generation System with Utilization of Unified Power Quality Conditioner

Noor Zanib[1], Munira Batool[1], Saleem Riaz[2], Farkhanda Afzal[3], Sufian Munawar[4], Ibtisam Daqqa[5] and Najma Saleem[5,*]

[1]Department of Electrical Engineering, University of Engineering and Technology, Taxila, 47050, Pakistan

[2]School of Automation, Northwestern Polytechnical University, 170072, Xi'an, China

[3]National University Science & Technology, MCS, Islamabad, 44000, Pakistan

[4]Department of Quantitative Methods, College of Business Administration, Imam Abdulrahman Bin Faisal University, Dammam, 34212, Saudi Arabia

[5]Department of Mathematics and Natural Sciences, College of Sciences and Human Studies, Prince Mohammad Bin Fahd University, Khobar, 31952, Saudi Arabia

*Corresponding Author: Najma Saleem. Email: nsaleem@pmu.edu.sa

Received: 27 January 2022 Accepted: 16 March 2022

ABSTRACT

This paper presents a comprehensive study that includes the sizing and power flow by series and parallel inverters in a distributed generation system (DGs) that integrates the system of hybrid wind photovoltaic with a unified power quality conditioner (UPQC). In addition to supplying active power to the utility grid, the system of hybrid wind photovoltaic functions as a UPQC, compensating reactive power and suppressing the harmonic load currents. Additionally, the load is supplied with harmonic-free, balanced and regulated output voltages. Since PV-Wind-UPQC is established on a dual compensation scheme, the series inverter works like a sinusoidal current source, while the parallel inverter works like a sinusoidal voltage source. Consequently, a smooth alteration from interconnected operating modes to island operating modes and vice versa can be achieved without load voltage transients. Since PV-Wind-UPQC inverters handle the energy generated through the hybrid wind photovoltaic system and the energy demanded through the load, the converters should be sized cautiously. A detailed study of the flow of power via the PV-Wind-UPQC is imperative to gain a complete understanding of the system operation and the proper design of the converters. Thus, curves that allow the sizing of the power converters according to the power flow via the converters are presented and discussed. Simulation results are presented to assess both steady state and dynamic performances of the grid connected hybrid system of PV-Wind-UPQC. This investigation is verified by simulating and analyzing the results with Matlab/Simulink.

KEYWORDS

Photovoltaic; wind turbine; unified power quality conditioner; power flow; distributed generation system

Nomenclature

C_p	Power coefficient

D_{V_s}	Voltage distortion power
D_L	Harmonic powers of the load
I_L	RMS load current
I_o	Saturation current of the diode
I_{ph}	Photocurrent
I_s	RMS grid current
L_{fpa}	Inductive filters of parallel NPC inverter
L_{fse}	Inductive filters of series NPC inverter
N_s	Number of series cells
P_{Bdc}	Active power absorbed through the DC bus
PF_{1L}	Fundamental power factor
P_L	Active load power
P_m	Mechanical output power
P_{pac}	Active parallel converter power
$P_{pv-wind}$	Active power generated through the PV array and Wind turbine
P_s	Active grid power
P_{sec}	Active series converter power
Q_L	Reactive powers of the load
R_{Lfpa}	Internal resistances of the parallel NPC inverter inductors
R_{Lfse}	Internal resistances of the series NPC inverter inductors
R_{sh}	Intrinsic shunt resistances of the PV cell
R_{se}	Intrinsic series resistances of the PV cell
S_L	Apparent load power
S_{pac}	Apparent parallel converter power
S_s	Apparent grid power
S_{s1}	Apparent fundamental grid power
S_{sec}	Apparent series converter power
THD_{V_s}	Total harmonic distortion of the grid voltages
THD_{i_L}	Total harmonic distortion of the load current
T_m	Output torque of the wind turbine
V_L	RMS load voltages
V_s	RMS grid voltage
V_t	Thermal voltage
V_w	Wind speed
ω_r	Rotor speed (rad/sec)
DG	Distributed generation
ESS	Energy storage systems
K	Boltzmann constant
MPPT	Maximum power point tracking
NPC	Neutral point clamped
P&O	Perturbs and observes
PCC	Point of common coupling
PI	Proportional-integral
PMSG	Permanent magnetic synchronous generator
PQ	Power quality
PV	Photovoltaics
q	Charge of the electron

R	Radius of the rotor blade
RESs	Renewable energy sources
T	Temperature in kelvin
UPQC	Unified power quality conditioner
WT	Wind turbine
λ	Speed-tip ratio
β	Pitch angle blade
ρ	Air density

1 Introduction

Global demand for electricity continues to grow. The two main electricity consuming sectors are residential-tertiary and industrial [1,2]. Today, the most reliable and resilient energy systems rely on the combustion of fossil fuels, which still dominate the world. In contrast, fossil fuels release greenhouse gases directly into the atmosphere and are not renewable. This had serious effects on the environment and human health. There are numerous alternate resources that may supply continuous, clean and renewable energy, for example: Wind, hydroelectric, geothermal, solar and biomass energy. Furthermore, renewable energy sources (RES) are getting great consideration around the world as a sustainable substitute energy source as a major part of global power production [3–8]. However, it is also the good way to recycle waste plastics and make energy collection and generation devices based on them. The triboelectric nanogenerator is one of them that is entirely based on waste plastic bags [9–13].

At present, RES based distributed generation systems (DG) are evolving as an substitute to huge decentralized traditional power systems associated to long electricity distribution/transmission systems [14]. Renewable energy sources based DG systems may be add on to latest electrical power systems to meet growing demand for electricity, reduction in costs of transmission of electricity, improve reliability of the system because of reducing the dangerous environmental effects of contaminating energy sources, for example: natural gas, oil, and coal and increased demand [15–18]. Injected in this scenario, photovoltaic and wind energy are the utmost extensively distributed renewable energy generation (DG). The weakness of wind turbines and photovoltaics, in addition to being able to generate electricity, creates a series of current and voltage harmonics caused through the existence of different sorts of photovoltaic devices and wind turbines and power inverters, In addition to the rise in the amount of non-linear loads associated to the network, it ultimately leads to a deterioration in the quality of the network [19,20].

When Photovoltaic systems is connected to three or single-phase electrical power systems, aim to supply a network with energy from photovoltaic assemblies [21–24]. An inverter stage is necessary as soon as the photovoltaic generator produces power in the form of direct current [25–34]. In contrast, a DC-DC boost converter must be required if the voltages in the DC bus of a photovoltaic array are not sufficient to provide the DC bus of the inverter phase [29–31]. This means that photovoltaic systems may be categorized as single or two stage energy conversion systems. In a system of single stage photovoltaic, maximum power point tracking (MPPT) monitoring must be done by a DC/AC converter [26,27], whereas in a system of two-stage photovoltaic, this job is typically accomplished via a DC/DC boost converter [32]. Whatever the topology of a photovoltaic system, the power balance between the system of photovoltaic and the electrical grid is achieved through regulating the voltages of DC bus of the inverter.

In various applications, the functionality of photovoltaic systems may be demonstrated. This occurs as photovoltaic systems, in addition to supplying the grid with active energy [15–31,35,36], can simultaneously perform a type of grid conditioning [31–35] and then improve the PQ indicators, which refer to the succeeding indices [37]: line utilization factor (fundamental Power factor (PF_{1L}) and power factor), load asymmetry factor and harmonic pollution factor.

In [31–34], photovoltaic systems operating in the same way just as the parallel active power filters which remove current harmonics generated by non-linear loads and compensate reactive power. In [38–41], photovoltaic systems were used to operate in an integrated fashion using UPQC [42–45]. Iterative control method is used to locate the specific position and time of the fault by its repetitive property. The data produced in each iteration is used for the next iteration for improvement in control system. The modeling of iterative control method for linear and non linear system is difficult work. The optimal control scheme based on optimization shows improves performance of the iterative control algorithm. For system optimization convergence speed of iterative control algorithm is important and is improved by applying optimal control scheme [46–51].

However the core task of the system of UPQC is to do parallel and series compensation as a result they may act instantaneously like a series active power filter (S-APF) compensating for line voltages, in addition to compensating the load currents as a parallel APF (P-APF) is used, in [38] experimental outcomes of the single-stage system of photovoltaic integrated with UPQC it simply fulfills the purpose of dynamic voltage restorer. In this situation, only mains voltage disturbances are compensated. In [39], computer simulations of the two-stage photovoltaic system called SPV-UPQC-P integrated with UPQC was presented. Although, this system simply compensates for imbalances grid voltage and reactive load power. Hence, the suppression of mains voltage and the harmonics of the load current have not been taken into account.

In [52], the UPQC, provided by the photovoltaic panels of the PI, boost converter, p-q theory, and the MPPT P and O, was presented. The system was capable to compensate for lessen source current/load voltage harmonics and reactive power however did not address intruption and reduction of sag caused via PV penetration.

In [53], migitation of power quality issues using UPQC on microgrid provided via wind turbine and PV has been proposed. It resulted that FLC and PI was capable to reduce distortion in output power and improve power quality. In [54], to overcome interruption voltage to grid and low sag to deliver active power, the wind turbine-UPQC has been presented. The system was using VSC like a rectifier on generator output and controlled so that required maximum energy may be produced through wind turbines (WT) at different speed by means of PI. In [55], the wind turbine-UPQC associated to UPQC DC link was executed. The presented combination with PI made it possible to compensate reactive power, interruption voltage and swell both on off/on utility grid. In [56], to enhance power quality in a grid coupled DFIG, wind turbine UPQC controlled by FLC have been proposed. FLC may enhance power quality, i.e., load current harmonics and sag voltage better than PI.

One more application wherein the photovoltaic model is integrating by using UPQC is presented in [40]. According to this application, the model may work as grid-forming in an AC micro-grid [36], in an island micro-grid, energy storage systems (ESS) and several kinds of DG sources (wind, photovoltaic and others) are using as grid-forming [57]. Though, when the system changes from grid-connected mode to the grid-islanded mode the disturbances/transients may be noticed in the voltages supplying the load. This occurs because of the UPQC parallel inverter requires to change its control mode to voltage source from current source. The similar result happens while the system returns to grid-tied operation, as the parallel inverter should be reactivated like a current source.

The system of PV-UPQC was presented in [41]. To compensate the supply voltage quality problems, i.e., harmonics, sag, flicker, threshold imbalance, and load current quality issues, i.e., neutral current, harmonics, reactive currents and imbalances UPQC is used. It may be work in both 3-Φ four -wire and 3-Φ three-wire electrical power systems. Meanwhile the parallel inverter is voltage controlled hence regulated voltages and balanced may be supplied to the load, it is not necessary to alter its control mode when the system works like a grid-forming in an AC micro-grid. In other words, the parallel inverter is voltage controlled both in grid islanded mode and in grid connected mode. In contrast, the mentioned system may also work in an AC micro-grid either as grid-supporting or grid-feeding [36], meanwhile the control mode of a parallel inverter may too be swapped to work to the current source from voltage source.

In contrast, the detailed studies on the apparent and active power flow and essentially the protection and sizing of the inverters that make up the system of PV-Wind-UPQC have not been dealt with in [41,58]. In doing so, additional research contributions are presented in this paper, as follows:

1. This article presents a inclusive study that includes the power flow by the system of PV-Wind-UPQC in order to gain a general understanding of how the system works in different modes of operation. This study signifies an essential and valuable methodological tool for properly designing the power inverters. It is based on an wide number of sizing curves and permits the designer an effective sizing of power converters.
2. Meanwhile the system of PV-Wind-UPQC simultaneously supplying the grid with active energy (energy generated by the photovoltaic and wind systems), in addition to the improvement of PQ indicators through series-parallel conditioning capabilities of power lines.

This article is structured as follows: Section 2 comprises the explanation of the system of PV-Wind-UPQC, the model of the PV and PMSG wind turbine and strategies for controlling the inverters in series and in parallel. Section 3 comprises complete explanations of the apparent and active power flows by PV-Wind-UPQC, resulting from standardized curves for the correct sizing of neutral point clamp (NPC) series and parallel inverters. In Section 4, the performance of the system in steady state and dynamic is evaluated based on the results of the simulation. Lastly, Section 5 presents the conclusions.

2 Explanation of the PV-Wind-UPQC Topology

The whole circuit diagram of the 3-Φ single-stage PV-Wind-UPQC system is presented in Fig. 1. The DGs based on RE sources, i.e., Hybrid PV-Wind coupled to 3P4W distribution system with 60 Hz frequency and 220 L-L volts via UPQC. The parallel and series inverters comprise of three-level NPC inverters. NPC inverter is a family of multi-level power inverters categorized through the usage of clamping diodes to ensure appropriate shared voltage between the power switches. The typical NPC stage features four IGBTs and six diodes. When using an NPC unit such as in the process of the converter, the voltage of dc link may be transformed into a variable AC voltage and a frequency. At the output, unlike a half-bridge or six-pack, a NPC strategy provides an extra voltage level. The potential does not just jump to DC+ and DC−: may also have 0 condition. The parallel converter is associated to the common coupling point 2 (PCC2) via an LC filters. The series converter is associated to the grid via three series-coupled transformers with L filters. The DC bus is consisting of the split-capacitor. The DGs, without storage, is consist of a PV array composed of a string with 20 series connected PV panels and a PMSG Wind Turbine.

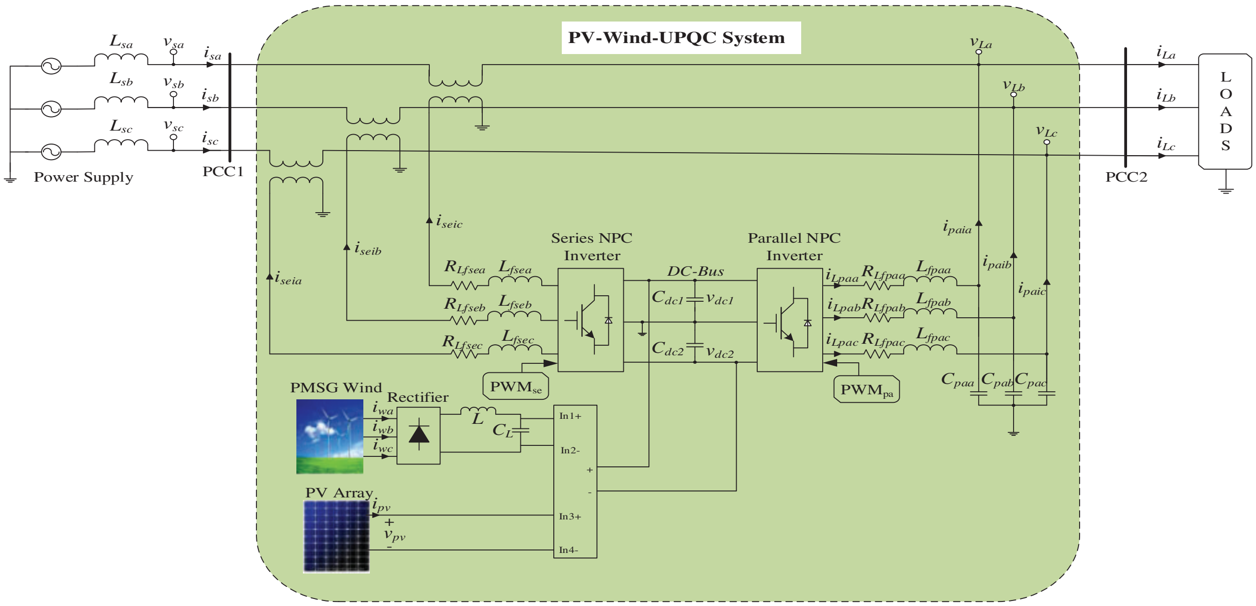

Figure 1: Power circuit of the system of PV-Wind-UPQC associated to a traditional electrical distribution system

The system of PV-Wind-UPQC is designed to work with the voltage reference of DC bus v_{dc}^{*}, which is determined through the MPPT algorithm [33]. Therefore, the maximum amplitude of the voltage of DC bus ($v_{dc\_max}^{*}$) is approximately 600 V, permitting the system to work in MPP on standard test conditions (STC). In contrast, the lowest working voltage of the system ($v_{dc\_min}^{*}$) is fixed at 460 V, i.e., when this voltage is reached the system works outside the MPP.

2.1 Photovoltaic Model

Fig. 2 displays the equivalent circuit diagram and the P-V and V-I curves of a solar module. A solar module comprises numerous photovoltaic cells which have outer connections in parallel, in series or in series-parallel [59].

In (1) the V-I featuers of a photovoltaic model is illustrated [60]:

$$I_{pv} = I_{ph} - I_o e^{\left(\frac{V_{pv}+R_{se}I_{pv}}{aV_t}-1\right)} - \frac{V_{pv} + R_{se}I_{pv}}{R_{sh}} \tag{1}$$

where I_o is the diode saturation current, I_{ph} is the photocurrent, a is ideal diode constant, $V_t = N_s KTq^{-1}$ is the thermal voltage, q s the charge of the electron, T is the temperature in Kelvin, N_s is the number of series cells, K is Boltzmann constant and R_{sh} and R_{se} are intrinsic shunt and series resistances of the photovoltaic cell, correspondingly.

Fig. 2 also shows the V-I and V-P relationship of photovoltaic modules. This figure clearly shows that the maximum power arises near the open circuit voltage of the photovoltaic module. A PV generator model is scaled for 20 modules in series and one parallel string (type: SW 245-SolarWorld). The nominal power of this panel is 245.168 W in STC state. The current at the maximum point and short-circuit current are 7.96 A and 8.49 A, correspondingly. The voltage at the maximum power and open circuit voltage are 30.8 volts and 37.5 volts, correspondingly.

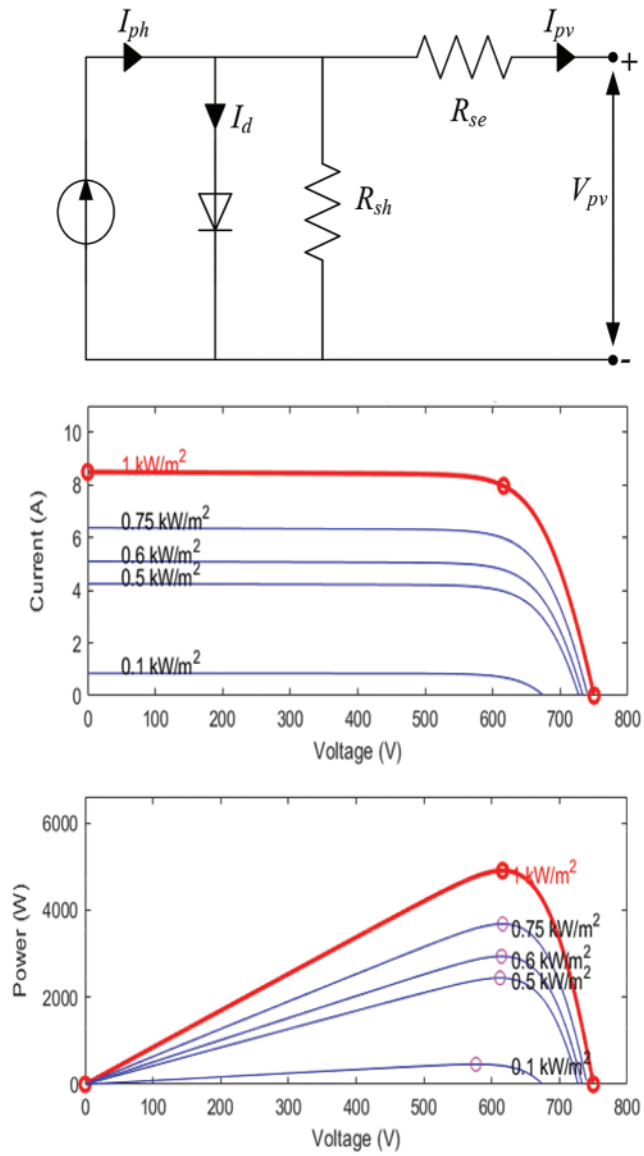

Figure 2: Equivalent circuit diagram and characteristic curve of the solar panel

2.2 PMSG Wind Turbine

The second source of energy in the DG construction is the wind turbine. A permanent magnet synchronous generators (PMSG) based wind power system is using to generate wind power. They may be categorized according to their operation: variable speed and fixed speed types [60]. In a fixed speed form, the rotational speed of the turbine is fixed and therefore the voltage generated frequency keeps constant thus this one may be associated straight to the grid. In this situation, every time the maximum power cannot be taken from the wind. In contrast, the turbine may revolve at varaince speeds, on variable speed, thus by using the MPPT method the maximum power may be produced at any wind speed [54]. Utilization of PMSG on a DFIG machine and a synchronous generator due to its consistency and high efficiency. With the removal of the outer rotor excitation, the price and size of the machine too decrease, being the PMSG easier to control with a system of feedback control. With variable speed wind turbine applications PMSG has turn into an smart solution for systems of wind power production [61]. Fig. 3 shows the model of PMSG wind turbine and it is power characteristics.

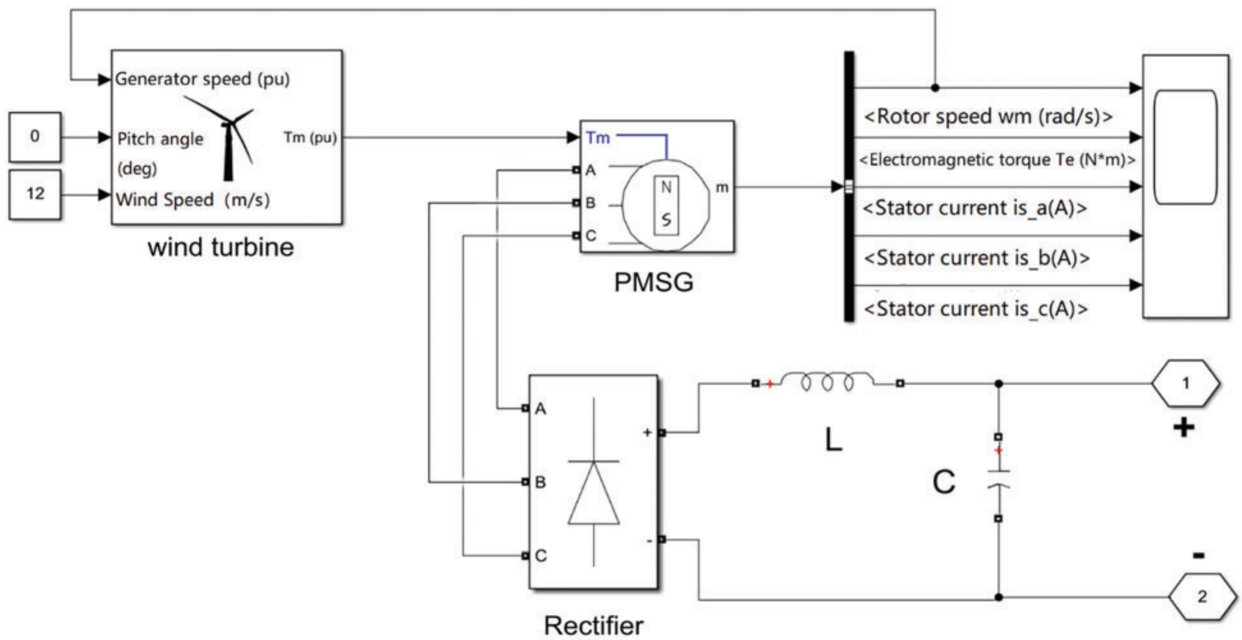

(a)

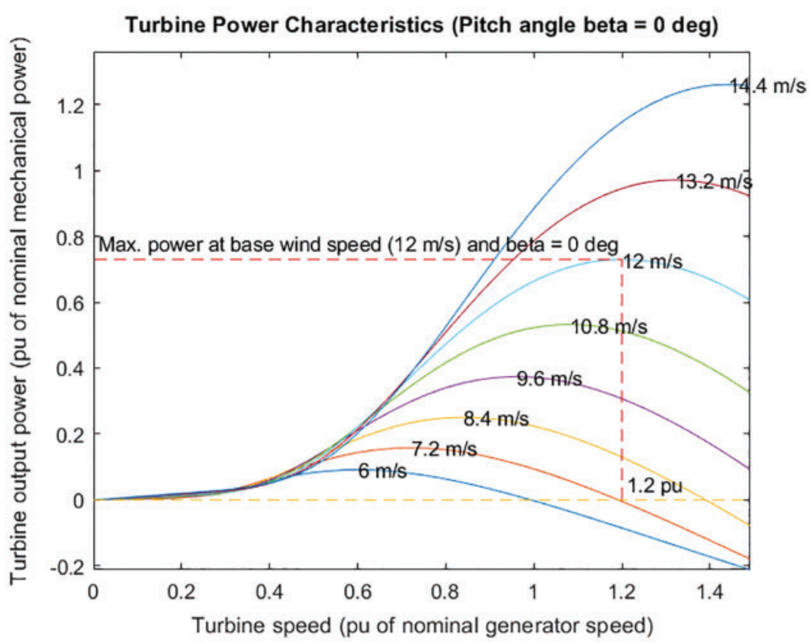

(b)

Figure 3: PMSG wind turbine model and it is power characteristics

The wind turbine output power may be stated by (2)–(4) [62].

$$\lambda = \frac{\omega_r R}{V_w} \tag{2}$$

$$P_m = \frac{1}{2}\rho C_p \pi R^2 V_w^3 \tag{3}$$

$$T_m = \frac{P_m}{\omega_r} = \frac{1}{2}\rho C_p \pi R^5 \frac{\omega_m^3}{\lambda^3} \tag{4}$$

Here λ is the speed-tip ratio, R is a radius of the rotor blade, V_w is the wind speed, ρ is the air density, ω_r is the rotor speed (rad/sec), P_m is the mechanical output power, T_m is wind turbine output torque and C_p is the power coefficient. The constant C_p depends on the value of pitch angle, on which rotor blade may revolve alongside axis and tip-speed ratio λ given in (5).

$$C_p = (0.44 - 0.167\beta)\, sin \frac{\pi\,(\lambda - 2)}{(13 - 0.3\beta)} \tag{5}$$

where pitch angle blade is represented by β. The value of β is adjust to a fixed value in a fixed pitch type. Table 1 illustrates all the parameters of PMSG.

Table 1: Parameters of PMSG

Parameters	Values
Stator phasor resistance	0.05 ohms
Armature Inductance	0.000635 H
Flux linkage established by magnets	0.192 V.s
Inertia	0.011 kg.m^2
Poles	4
Viscous damping	0.001889 N.m.s

2.3 Control Strategy of the System of PV-Wind-UPQC

The UPQC is generally controlled with a traditional compensating scheme in which the parallel inverter performs like a non-sinusoidal current source and the series inverter like a non-sinusoidal voltage source. However the dual compensation scheme is applied here to the UPQC varies from the traditional compensation scheme, in which the parallel inverter behaves like a sinusoidal voltage source, i.e., the output voltages of the system of PV-Wind-UPQC are controlled to be in phase and synchronized with the main voltages. Hence, to enable the flow of these currents by the parallel inverter a low impedance pathway is formed for the load harmonic currents. Meanwhile the system output voltages are controlled in a regulated, sinusoidal and symmetrical manner, all disturbances in the network, i.e., voltage asymmetries, voltage harmonics and voltage dips/over voltages, occur through the terminals of the series-coupled transformers.

The PV-Wind-UPQC input currents are regulated according to the main voltages. These currents are controlled through the series inverter so that a series inverter works as a symmetrical sinusoidal current source. This creates a higher impedence pathway for load harmonic currents between the load and grid, so as to a series inverter acts like a harmonic isolator. Subsequently the currents of grid are in phase and sinusoidal with the voltages of grid, no reactive or harmonic power circulates in the grid(PCC1).

Hence, a high power factor is achieved along with compensating for load imbalances. The voltages of DC bus regulator regulates the amplitude of grid currents so that the equilibrium of energy flow among the load, grid and the system of PV-Wind is achieved [58].

In this paper, the algorithms for generating the grid currents references (NPC series inverters), output voltages (NPC inverters in parallel) and voltage of DC bus (MPPT-P & O) are implemented in the synchronous reference frame (SRF) as presented in Figs. 4a and 4b. The mathematical modeling of inverters, these particular algorithms, voltage controllers (DC bus and parallel converter) in addition to current controllers (series converters) are shown in detail in [41,58]. The phase locked loop (PLL) strategy, that is utilized for the useful detection and synchronization of the phase angle, is described in [63].

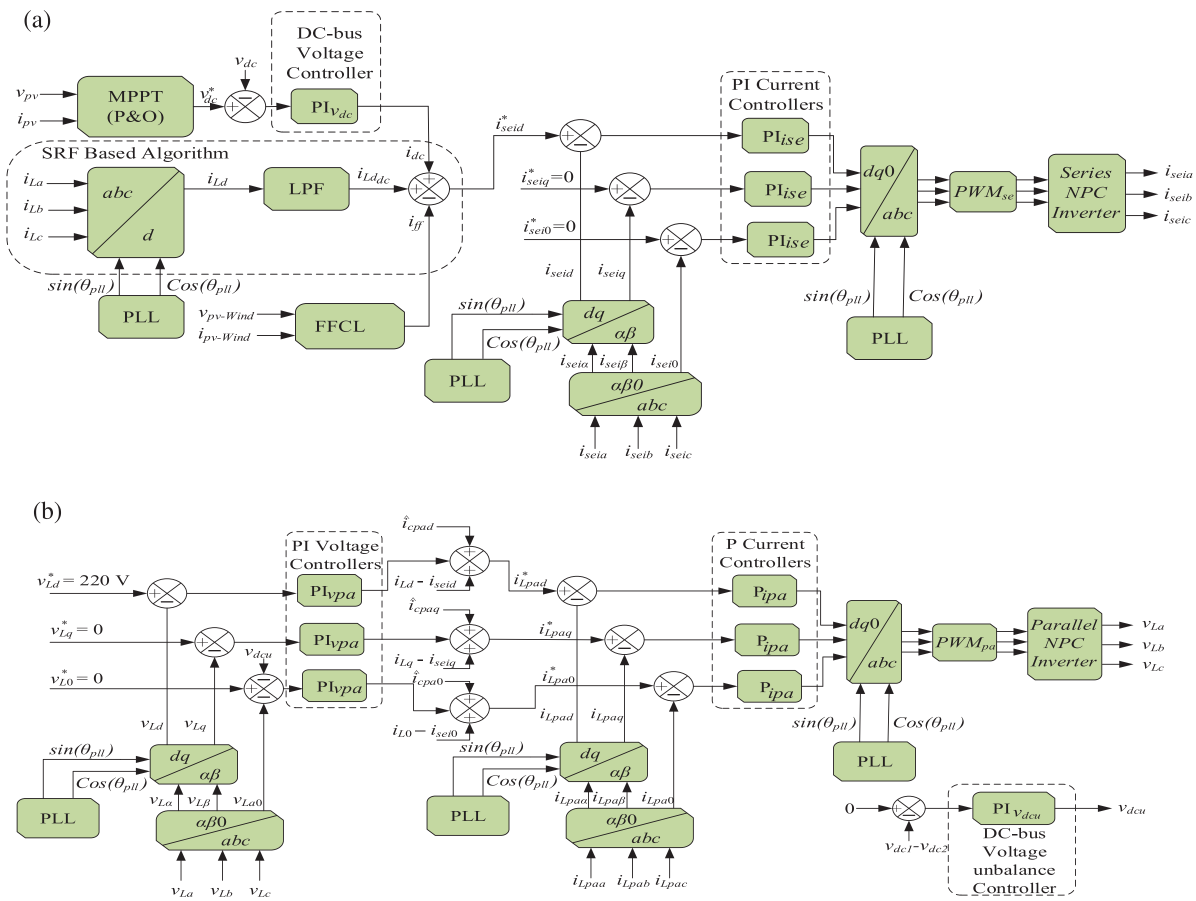

Figure 4: Serial and parallel inverter NPC control loop signal flow diagrams: (a) Series currents reference generation and control loops; (b) Parallel control loops and reference voltages generation

3 Power Flow by the Converters of the System of PV-Wind-UPQC

This segment describes the quantitative study of the power flows by the parallel and series inverters of the system of PV-Wind-UPQC. The following steady state system conditions are assumed for analysis:

1) The currents withdrawn from the grid are symmetrical and sinusoidal.
2) Voltages of grid are symmetrical, while they may comprise harmonics.

In addition to a clearly understand the system functionality, this study aims to provide subsides for the adequate sizing of parallel and series inverters. The subsides is carried out through curves where the two inverters apparent powers are standardized according to the total load apparent power. In specific, the apparent powers associated in energy flow by parallel and series NPC inverters based on the charcteristics of the load, grid and power generated via the photovoltaic generator and the PMSG wind turbine. These properties are described below:

1. The ratio between the RMS voltages of grid and load (V_s/V_L).
2. Fundamental power factor of the load (PF_{1L}).
3. Total harmonic distortion of the load currents (THD_{i_L}) and grid voltages (THD_{V_s}).
4. To compensating the system losses, the active power is consumed through the DC bus (P_{Bdc}), such as, losses in passive filtering components and switching components.
5. The active energy generated through the photovoltaic and PMSG wind turbine energy system ($P_{pv-wind}$).

3.1 Apparent Power of the Series Converter

The (6) illustrates the apparent complex power of series converter

$$\dot{S}_{sei} = \dot{V}_{SCT}\dot{I}_s^* \tag{6}$$

where $\dot{V}_{SCT} = \dot{V}_s - \dot{V}_L$ are RMS complex voltages in the series coupling transformer; and $\dot{I}_s^*$ is complex conjugate of RMS mains currents.

It is assumed that the RMS values of the mains voltage consists of fundamental and harmonic constituents denoted by V_{s1} and V_{sH}, respectively. Thus, series inverter apparent complex power is stated by:

$$|S_{sei}| = \sqrt{[(V_{s1} - V_L)\, I_s]^2 + (V_{sH} I_s)^2} \tag{7}$$

where the term $V_{sH}I_s$ characterizes the voltage distortion power, which is defined in [37] by:

$$D_{V_s} = V_{sH}I_s = V_{s1}I_sTHD_{V_s} = S_{s1}THD_{V_s} \tag{8}$$

where S_{s1} represents the fundamental apparent power of the grid.

Substituting (8) in (7) and by rearranging, results in:

$$|S_{sei}| = \sqrt{\left[V_{s1}I_s\left(1 - \frac{V_L}{V_{s1}}\right)\right]^2 + \left(S_{s1}THD_{V_s}\right)^2} \tag{9}$$

Considering that $S_{s1} = P_L$, and (10) can be rewritten as:

$$|S_{sei}| = \sqrt{P_L^2\left[\left(1 - \frac{V_L}{V_{s1}}\right)^2 + \left(THD_{V_s}\right)^2\right]} \tag{10}$$

Here, P_L is the real power needed via the load.

Supposing the load voltages balanced and sinusoidal, the load complex apparent power and the total load power factor will be $|S_L| = \sqrt{P_L^2 + Q_L^2 + D_L^2}$ and $PF_L = \frac{P_L}{S_L} = \frac{PF_{1L}}{\sqrt{1 + THD_{iL}^2}}$, respectively, where Q_L is the reactive and D_L is the load harmonic powers.

By standardizing $|S_{sei}|$ according to $|S_L|$, results in:

$$\frac{|S_{sei}|}{|S_L|} = \frac{PF_{1L}\sqrt{\left[\left(1-\frac{V_L}{V_{S1}}\right)^2 + THD_{VS}^2\right]}}{\sqrt{1+THD_{iL}^2}} \tag{11}$$

The apparent fundamental power of the grid is calculated through:

$$S_{s1} = P_{Total} = P_L + (P_{Bdc} - P_{pv-wind})/3 \tag{12}$$

$$S_{s1} = P_L + \left(1 + C_{Bdc} - C_{pv-wind}\right) \tag{13}$$

$$C_{Bdc} = P_{Bdc}/3P_L \tag{14}$$

$$C_{pv-wind} = P_{pv-wind}/3P_L \tag{15}$$

where P_{Bdc} is the active energy consumed via the DC bus and $P_{pv-wind}$ is the active energy genertaed by PV-wind energy system.

Thereby, by substituting (13)–(15) in (9), $\frac{|S_{sei}|}{|S_L|}$ is obtained as follows:

$$\frac{|S_{sei}|}{|S_L|} = \frac{PF_{1L}\sqrt{\left(1 + C_{Bdc} - C_{pv-wind}\right)^2\left[\left(1-\frac{V_L}{V_{S1}}\right)^2 + THD_{VS}^2\right]}}{\sqrt{1+THD_{iL}^2}} \tag{16}$$

3.2 Apparent Power of the Parallel Converter

The apparent complex power of the Parallel inverter is shown by:

$$\dot{S}_{pai} = \dot{S}_L - \dot{V}_L\dot{I}_s^* \tag{17}$$

Assume that the line currents are in phase and sinusoidal with the respective line voltages, and supposing that $S_{s1} = P_L$, the parallel converter complex apparent power can be calculated by:

$$|S_{pai}| = \sqrt{P_L^2 + Q_L^2 + D_L^2} - P_L\left(\frac{V_L}{V_{s1}}\right) \tag{18}$$

After some mathematical manipulating in (18), $|S_{pai}|$ is found as:

$$|S_{pai}| = \sqrt{P_L^2\left[\left(\frac{V_L}{V_{s1}}\right)^2 - 2\left(\frac{V_L}{V_{s1}}\right) + \frac{1+THD_{iL}^2}{PF_L^2}\right]} \tag{19}$$

By normalizing $|S_{pai}|$ according to $|S_L|$, $\frac{|S_{pai}|}{|S_L|}$ can be obtained as:

$$\frac{|S_{pai}|}{|S_L|} = \sqrt{\frac{PF_{1L}^2\frac{V_L}{V_{s1}}\left[\frac{V_L}{V_{s1}} - 2\right]}{1+THD_{iL}^2} + 1} \tag{20}$$

By including the active power P_{Bdc} and $P_{pv-wind}$ into the analysis, the above equation can be rewritten as:

$$\frac{|S_{pai}|}{|S_L|} = \sqrt{\frac{PF_{1L}^2 \frac{V_L}{V_{s1}} \left(1 + C_{Bdc} - C_{pv-wind}\right) \left[\frac{V_L}{V_{s1}} \left(1 + C_{Bdc} - C_{pv-wind}\right) - 2\right]}{1 + THD_{iL}^2} + 1} \tag{21}$$

3.3 Apparent Power Standardized Curves of the Series and Parallel Converters

The total load apparent power based on the normalized curves of apparent power of the series and parallel NPC inverters, i.e., $\frac{|S_{sei}|}{|S_L|}$ and $\frac{|S_{pai}|}{|S_L|}$ are demonstrated in Fig. 5.

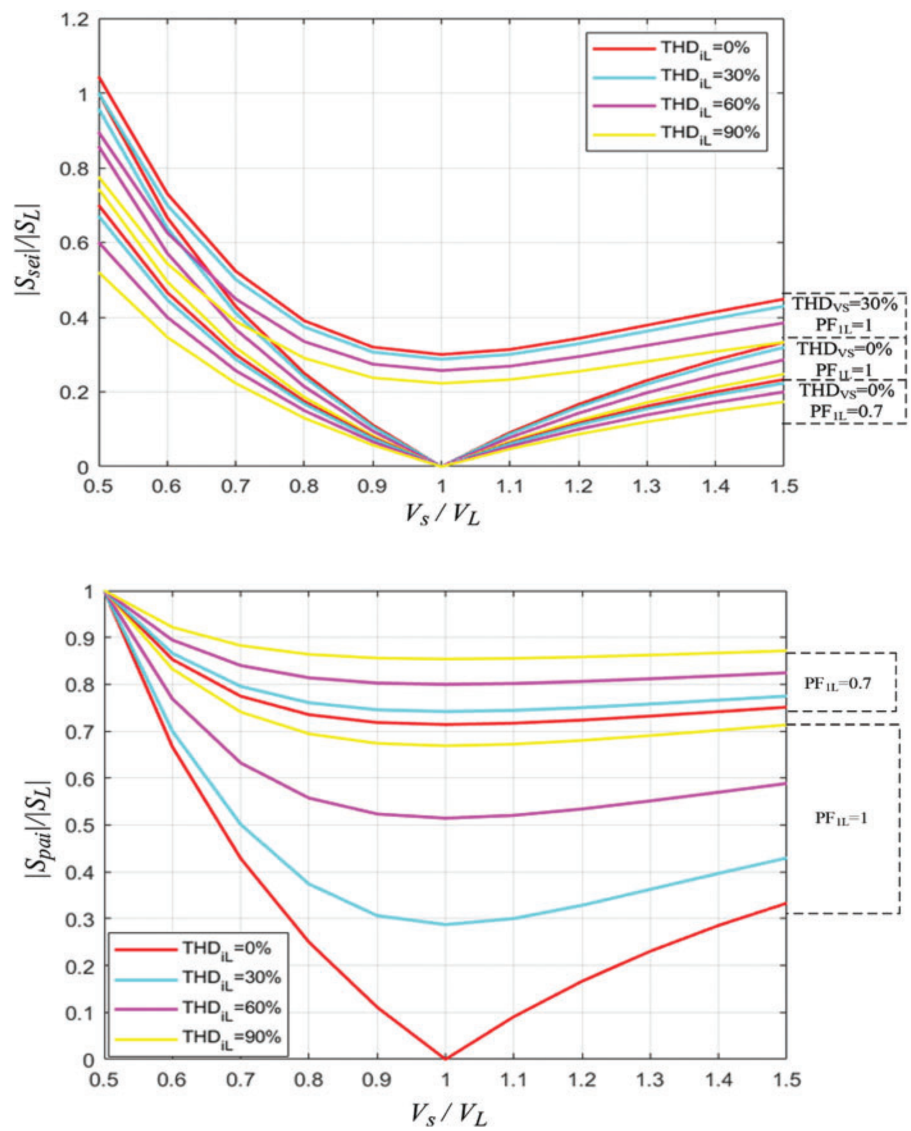

(a)

Figure 5: (Continued)

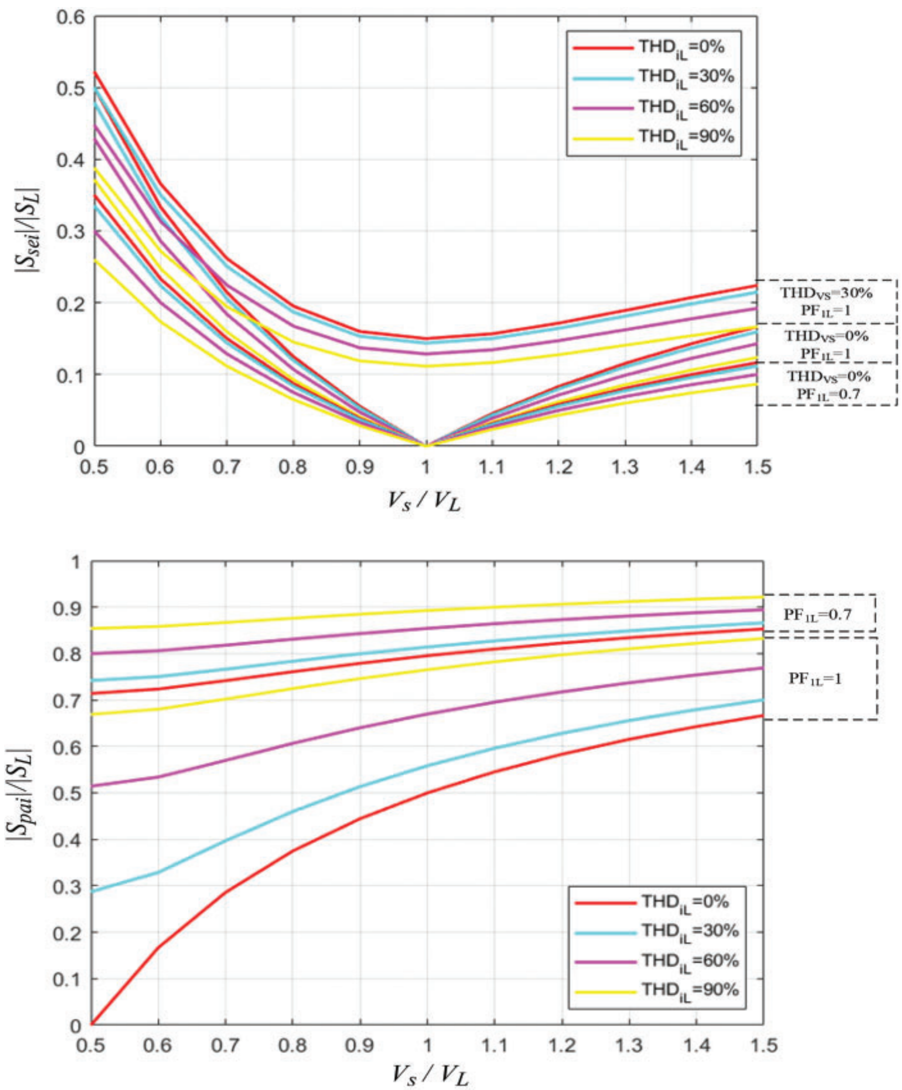

(b)

Figure 5: (Continued)

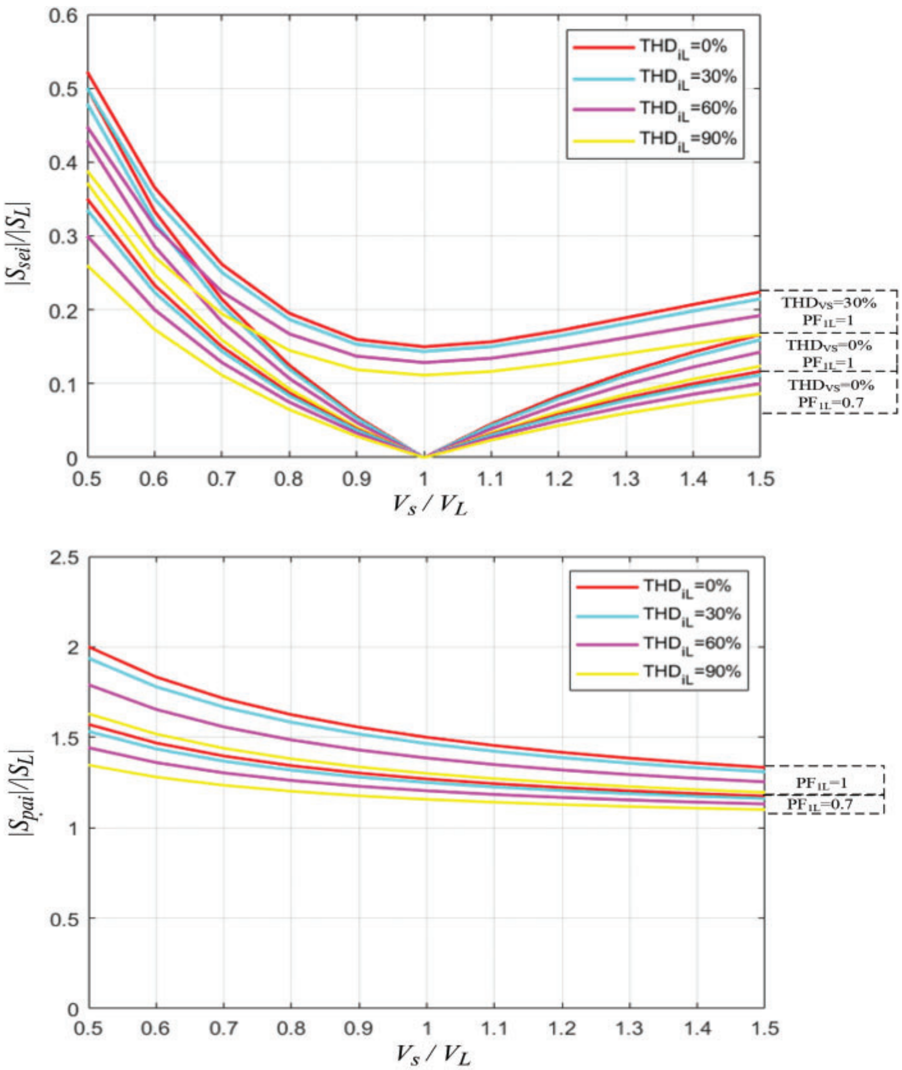

(c)

Figure 5: (Continued)

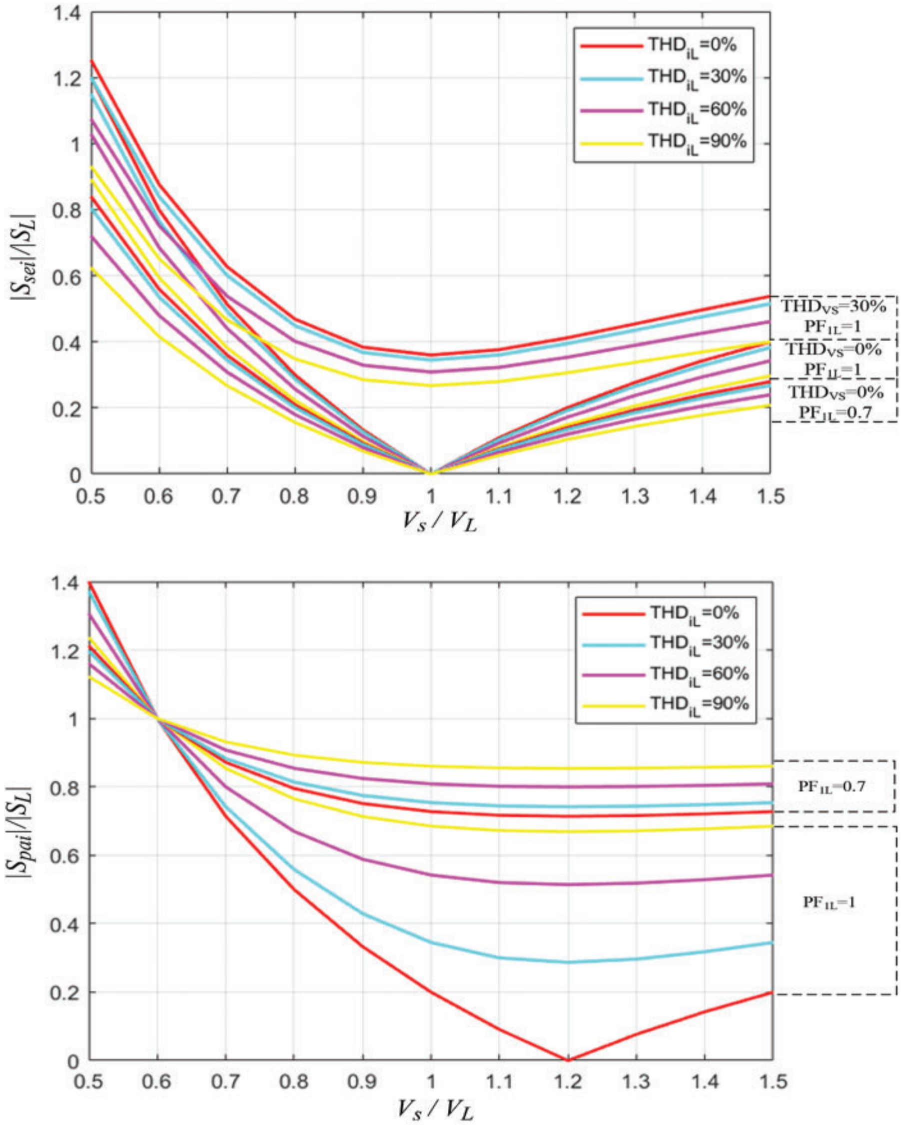

(d)

Figure 5: Normalized curves of the apparent power of series and parallel converters: (a) $\frac{|S_{sei}|}{|S_L|}$ and $\frac{|S_{pai}|}{|S_L|}$ for $C_{Bdc} = 0$ and $C_{pv-wind} = 0$; (b) $\frac{|S_{sei}|}{|S_L|}$ and $\frac{|S_{pai}|}{|S_L|}$ for $C_{Bdc} = 0$ and $C_{pv-wind} = 0.5$; (c) $\frac{|S_{sei}|}{|S_L|}$ and $\frac{|S_{pai}|}{|S_L|}$ for $C_{Bdc} = 0$ and $C_{pv-wind} = 1.5$; (d) $\frac{|S_{sei}|}{|S_L|}$ and $\frac{|S_{pai}|}{|S_L|}$ for $C_{Bdc} = 0.2$ and $C_{pv-wind} = 0$

Fig. 5a, displays the normalized apparent power curves taking into account the factors $C_{Bdc} = 0$ and $C_{pv-wind} = 0$. For $THD_{V_s} > 0$, the power processed by series converter rises over the whole range covered by the $\dfrac{V_s}{V_L}$ proportion, i.e., $0.5 < \dfrac{V_s}{V_L} < 1.5$. With $THD_{V_s} = 0$, the energy processes only if the ratio $\dfrac{V_s}{V_L} \neq 1$. In Fig. 5a, from the curve $\dfrac{|S_{pai}|}{|S_L|}$ the following rule applies: the higher the THD_{i_L} and the lower the PF_{1L}, the better the performance of the parallel inverter.

Fig. 5b shows the normalized power curves taking into account $C_{Bdc} = 0$ and $C_{pv-wind} = 0.5$. In this situation, 50% of entire active power spent through the load is supplied through the photovoltaic array and the PMSG wind turbine. The curves shown in Fig. 5b, thus verify that the lesser power extracted from the utility grid, the lesser power handled through the series inverter. This means that all or maximum of the active power produced through the PV generator and PMSG wind turbine goes through parallel converter, Fig. 5b illustrates an rise in the processed power through the mentioned inverter for this state of functioning.

Fig. 5c illustrates the normalized power curves for condition $C_{pv-wind} = 1.5$, where $P_{pv-wind} > P_L$. In this condition, the active power fed into the utility grid corresponds to 50% of the active power spent through the load. If you compare the graphs in Figs. 5b and 5c, the series inverter processes the similar power in both situations, irrespective of the way of the active power flow. However, according to the normalized curves, dependent on the $\frac{V_s}{V_L}$ ratio, the parallel inverter processes entire active power produced through the photovoltaic system and the PMSG wind turbine. In addition, portion of this energy is made available to consumer and the remaining is inserted into the utility grid.

Fig. 5d shows the normalized curves taking into account $C_{Bdc} = 0.2$ or $C_{pv-wind} = 0$. In this situation, it is supposed that the active power is taken from the utility grid to control the voltage of DC bus in order to keep the power balance of a system. Hence, the power handled through series inverter rises while $\frac{V_s}{V_L} \neq 1$ or $THD_{V_s} > 0$, as shown in Fig. 5d. Furthermore, at certain places of the curves $\frac{|S_{pai}|}{|S_L|}$ as presented in Fig. 5d, a rise in the power handled through parallel inverter may be also noticed, such as, in a state $\frac{V_s}{V_L} = 1$, $THD_{i_L} = 0\%$ and $PF_{1L} = 1$. On the other hand, the stated active power may be handled through each of inverters (parallel or series) or both at the same time, depending on the $\frac{V_s}{V_L}$ ratio.

3.4 Active Power Flow by the System of PV-Wind-UPQC

Figs. 6 and 7 illustrate the instant active power flow by the inverters that comprise the system of PV-Wind-UPQC. The directions of power flow are governed by the following characteristics:

1) Difference between the RMS voltages of the grid (V_s) and of the load (V_L).
2) Quantity of energy consumed through the load.
3) Quantity of energy generated through the photovoltaic array.

The instantaneous active powers included in the analysis are described below: grid power (P_s), power of photovoltaic array and wind turbines ($P_{pv-wind}$), power of series inverter (P_{sei}), power of parallel inverter (P_{pai}) and load power (P_L). This analysis does not include losses in passive components of the system of PV-Wind-UPQC or the switching components of the NPC converters, i.e., the investigation takes into account $C_{Bdc} = 0$. Table 2 illustrates all of the operative conditions for determining the active power flow by the converter.

1) Operating Condition 1: $V_s > V_L$

a) Fig. 6a describes the energy flow by the system of PV-Wind-UPQC for $P_{pv-wind} = 0$ W. In this senario, whole real load power is taken from the grid. When $V_s > V_L$, portion of the energy passes to the series converter from the utility grid and to the load from the parallel converter.

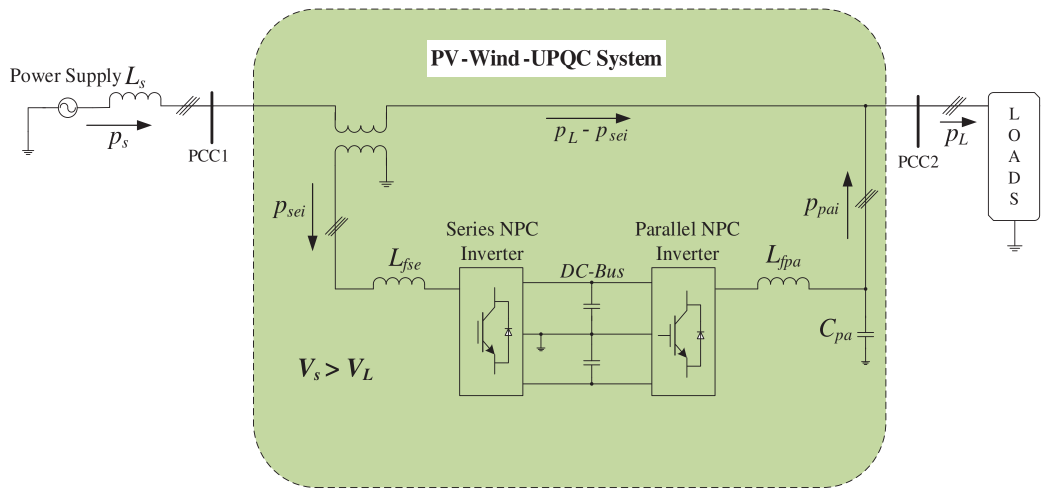

(a)

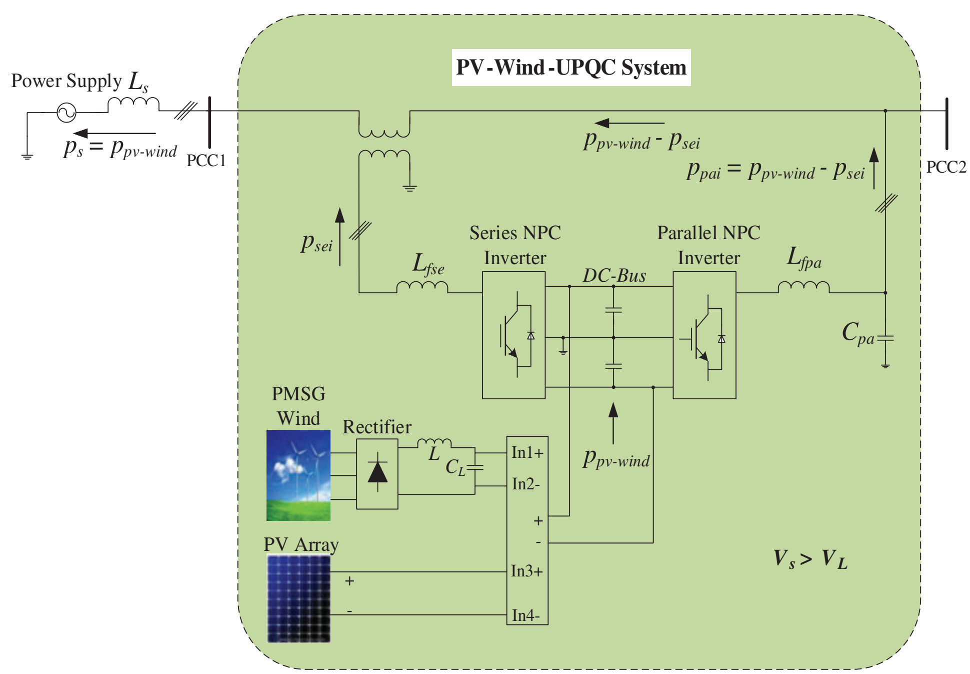

(b)

Figure 6: (Continued)

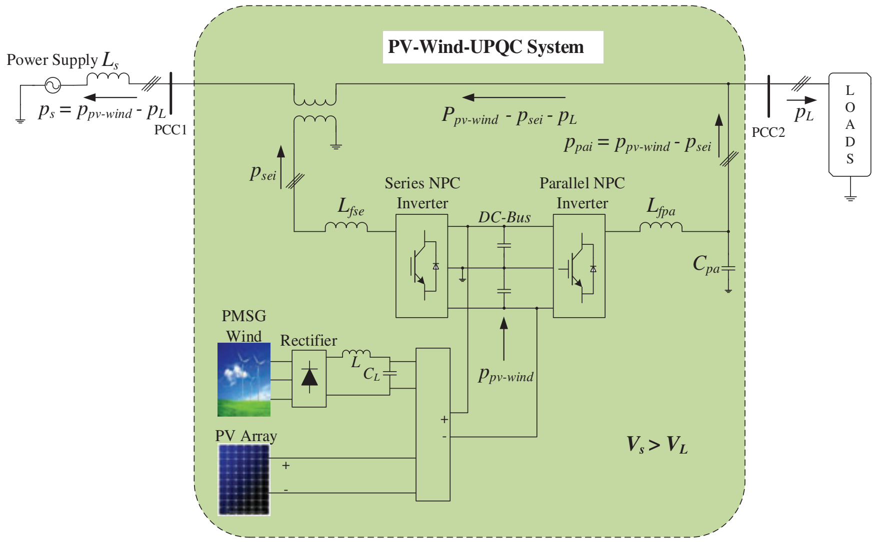

(c)

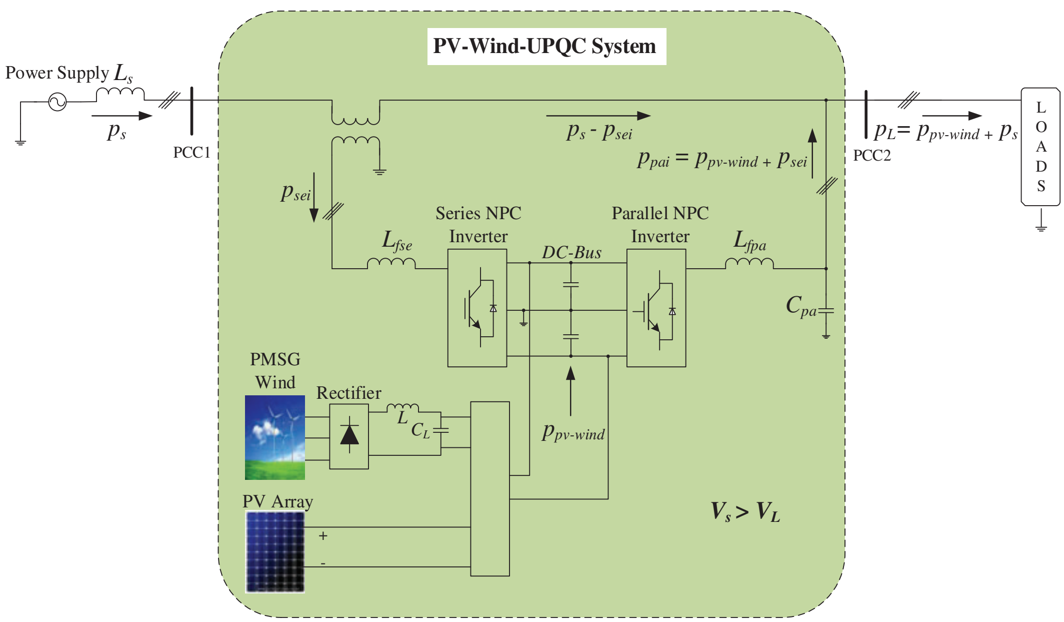

(d)

Figure 6: Flow of active power by the PV-Wind-UPQC: Condition 1: $V_s > V_L$; (a) $P_L \neq 0$ and $P_{pv-wind} = 0$; (b) $P_L = 0$ and $P_{pv+wind} > 0$; (c) $P_{pv-wind} > P_L$; (d) $P_{pv-wind} < P_L$

b) In Figs. 6b–6d, assume that $P_{pv-wind} \neq 0$ W. In Fig. 6b, we can see that at $P_L = 0$ W, all the power produced through the photovoltaic and wind energy system is fed into a grid via the two inverters. It should also be noted that maximum of this energy is still handled via the parallel inverter.

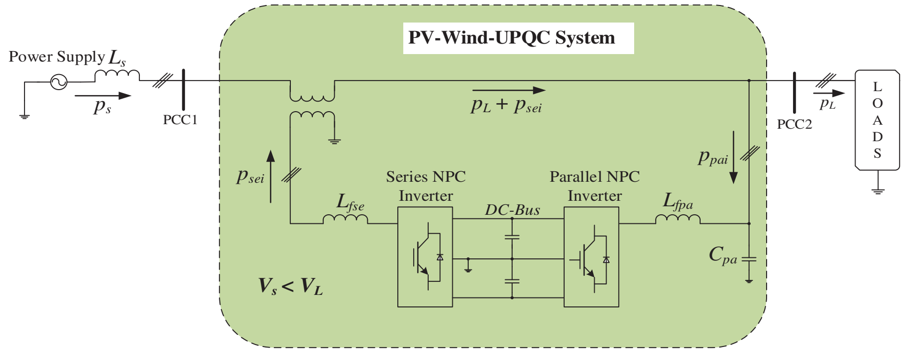

(a)

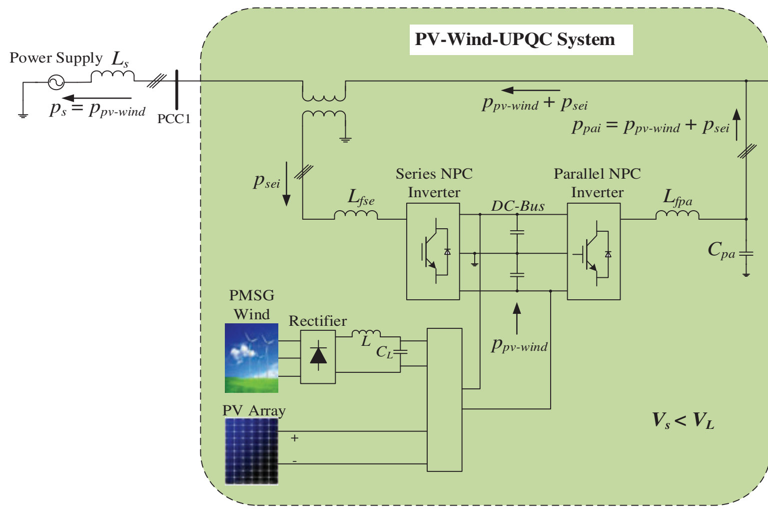

(b)

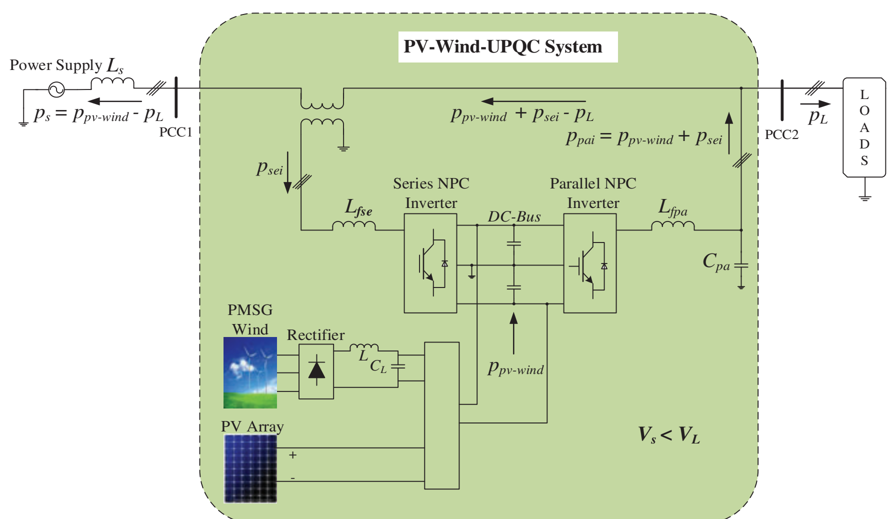

(c)

Figure 7: (Continued)

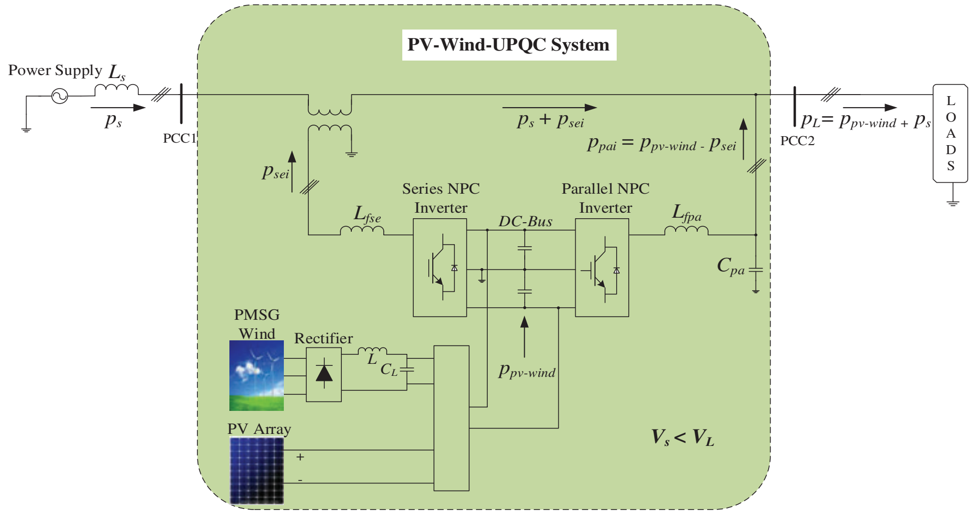

(d)

Figure 7: Flow of active power by the PV-Wind-UPQC: Condition 2: $V_s < V_L$; (e) $P_L \neq 0$ and $P_{pv-wind} = 0$ (f) $P_L = 0$ and $P_{pv-wind} > 0$; (g) $P_{pv-wind} > P_L$; (h) $P_{pv-wind} < P_L$

Table 2: Operating conditions assumed to regulate the flow of active power by the PV-Wind-UPQC system

Conditions		RMS voltages	Load power	Power of PV and wind
	a		$P_L \neq 0$	$P_{pv-wind} = 0$
1	b	$V_s > V_L$	$P_L = 0$	$P_{pv-wind} > 0$
	c		$P_L > 0$	$P_{pv-wind} > P_L$
	d		$P_L > 0$	$P_{pv-wind} < P_L$
	a		$P_L \neq 0$	$P_{pv-wind} = 0$
2	b	$V_s < V_L$	$P_L = 0$	$P_{pv-wind} > 0$
	c		$P_L > 0$	$P_{pv-wind} > P_L$
	d		$P_L > 0$	$P_{pv-wind} < P_L$

c) In Fig. 6c, assume that $P_L \neq 0$ and $P_{pv-wind} > P_L$. In this senario, portion of the energy produced through the photovoltaic generator and the wind turbine is fed into the grid via the inverters in parallel and in series, whereas the remaining energy is supplied to the load via the parallel inverter.

d) In Fig. 6d, assume that $P_L \neq 0$ and $P_{pv-wind} < P_L$. In this situation, entire energy generated through the photovoltaic and wind energy system is made available to the consumer through parallel inverters, whereas the remaining power is taken from the utility grid. It may be noted that portion of the energy supplied through the grid passes by both parallel and series converters.

2) *Operating Condition 2:* $V_s < V_L$

a) Fig. 7a describes the energy flow by the system of PV-Wind-UPQC for $P_{pv-wind} = 0$ W. In this senario, whole real load power is taken from the utility grid. Comparison of Figs. 7a and 6a. If $V_s < V_L$, the way of the flow of energy changes.

b) In Figs. 7b–7d, assume that $P_{pv-wind} \neq 0$ W. In Fig. 7b, with $P_L = 0$ W, whole energy prduced via the photovoltaic wind energy system is transferred to the utility grid via the parallel converter. Furthermore, the real power flowing via the series converter also passes via the parallel converter.

c) In Fig. 7c, assume that $P_{pv-wind} > P_L$ and $P_L \neq 0$ W. In this senario, portion of the energy generated through the energy system of photovoltaic-wind is routed to utility grid via parallel converter, whereas the rest of the energy is routed to the consumer. As may be seen, the real power also goes via the series converter.

d) In Fig. 7d, $P_L \neq 0$ W and $P_{pv-wind} < P_L$. In this senario, the power produced by the photovoltaic wind energy system is supplied to the load via parallel and series converters, whereas the left over power is taken from the utility grid.

In an ideal sitaution, when $V_s = V_L$, there is no flow of active power via the series converter, as shown in the curves presented by Figs. 5a–5d.

3.5 Sizing Examples of Series and Parallel Converter

In this section some examples are made for the sizing of parallel and series inverters, taking into account three operating conditions of the system of PV-Wind-UPQC that are based on the power flow analysis presented above. With such sizing, it is taken into account that the load is associated to the system and that the active energy consumes $P_L = 1000$ W per phase. Table 3 compiles the values assumed for the sizing of parallel and series inverters.

Table 3: Operating states assumed for scaling parallel and series converter

Operating states	V_s/V_L	$C_{pv-wind}$	C_{Bdc}	PF_{1L}	THD_{V_s}	THD_{i_L}	$\|S_L\|$ (VA)	$\|S_{sei}\|$ (VA)	$\|S_{sei}\|/\|S_L\|$	$\|S_{pai}\|$ (VA)	$\|S_{pai}\|/\|S_L\|$
1	1	2	0	1	0%	0%	1000	0	0	2000	2
2	0.75	0	0	1	15%	0%	1000	365.22	0.365	333.33	0.333
3	0.75	2	0	1	15%	100%	1207.1	311.98	0.258	2166.79	1.795

In the primary operating state, an ideal situation is considered. In this case, it is assumed that the photovoltaic and wind energy system, which are connected to the DC bus, have maximum production capacity, e.g., double the active power spent by the load, hence $C_{pv-wind} = 2$. This ensures that whole the active energy drawn from the photovoltaic and wind energy system is processed via the parallel inverter.

This converter must therefore be dimensioned by considering the maximum active energy of the photovoltaic and wind energy system. Therefore, the sizing of this converter must be carried out by considering the maximum active power being delivered through wind and photovoltaic energy system.

In secondary operating state, it is considered mains voltages having a great harmonic content ($THD_{V_s} = 15\%$) and an operation of the system with a voltage drop of 25%. From the Table 3, it is clear that the series inverter may be designed for a rated power lesser than 40% of the rated power of the load, also taking into account the operation of the grid in voltage disturbances (sag/harmonics). Thus, it is obvious that the lower energy level processed via the serial inverter is a greater benefit for the system of PV-Wind-UPQC. In contrast, it was found that the parallel inverter also handles power with $THD_{i_L} = 0\%$ and $PF_{1L} = 1$, since $V_s/V_L \neq 1$. However, when sizing this converter, voltage drops should be taken into account.

In the tertiary state of operation, the load currents are assumed to have higher harmonic components, such that: $THD_{i_L} = 100\%$. It is also considered that $PF_{1L} = 1$, $THD_{V_s} = 15\%$, $V_s/V_L = 0.75$ and $C_{pv-wind} = 2$. If you compare this operating state with above presented two states, you can see that the power handled through the parallel inverter rises, which shows that the sizing of this inverter must be taken into account the reactive power spent through the load.

4 Simulation Results

The performance of PV-Wind-UPQC is assessed through simulating the system in software of MATLAB/Simulink. Complete system parameters and the three-phase non-linear load are presented in Appendix. Sinusoidal Pulse Width Modulation (SPWM) strategy is utilized in series and parallel NPC inverters [64].

4.1 Static Results

This segment describes simulation results in which the PV-Wind-UPQC is operated in three operating modes (OPM). Such OPMs are depicted in Figs. 8–10, taking into account various operating conditions to which the PV-Wind-UPQC is exposed. The OPM 1, arises when the local load associated to the system of PV-Wind-UPQC needed solar irradiance instantaneous power, so that $P_{pv-wind} > P_L$. In OPM 2, which takes place at night time (without solar radiation), the system works simply in PV-Wind-UPQC, so that $P_{pv-wind} = 0$ W. Finally, in OPM 3 the system of PV-Wind-UPQC works without load and simply supplies the grid with real power.

4.1.1 Performance of PV-Wind-UPQC at $P_{pv-wind} > P_L$

Fig. 8, shows the power system of PV-wind-UPQC which is operating with the balance 3-Φ nonlinear load while processing the power of photovoltaic and wind energy system. Now in that case the power of photovoltaic and wind turbine ($P_{pv-wind} \cong 3500$ W) is more as compare to the active power needed through load (P_L) and $V_s \cong V_L$. Therefore, the system supplies active energy to the grid along with the active conditioning of the power lines in series and in parallel. As may be seen, the real power needed by the load is supplied in full through the photovoltaic-wind energy system and the excess active power generated is fed into the utility grid via the parallel converter. It should also be noted that the flow of active energy by the series inverter with $V_s \cong V_L$ is too much low. It is also noted that the currents of grid are in opposite phase and sinusoidal with the utility grid voltages.

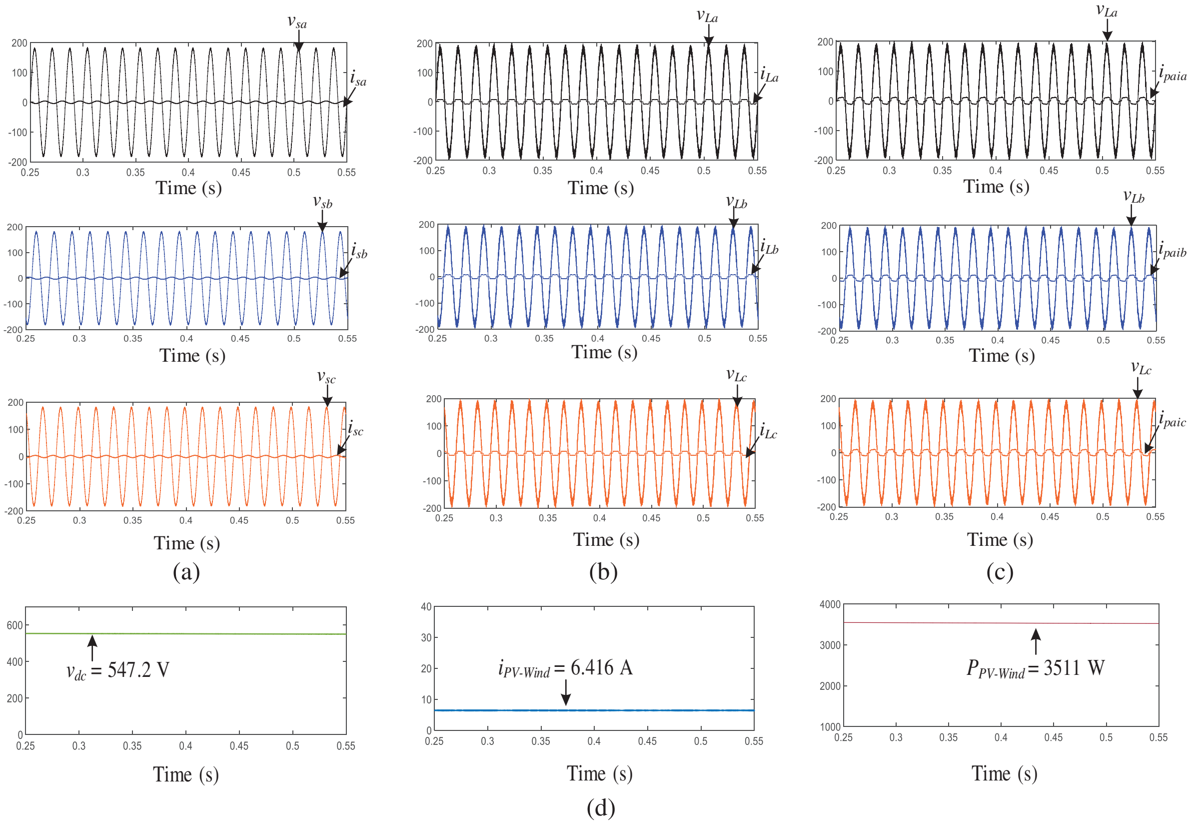

Figure 8: OPM 1: Active power-line conditioning along with active power interjection is performing by PV-Wind-UPQC ($P_{pv-wind} > P_L$ and $V_s \cong V_L$): (a) waveforms of the phase 'a, b and c' grid current and voltages; (b) waveforms of the phase 'a, b and c' load current and voltages; (c) waveforms of the phase 'a, b and c' parallel NPC inverter current and voltages; (d) waveforms of voltages of DC bus $i_{pv-wind}$ current; and power generated via PV and Wind energy system

4.1.2 Performance of PV-Wind-UPQC at $P_{pv-wind} = 0$ W

The results presented in Fig. 9 are attained with the system of PV-Wind-UPQC that is functioning as UPQC (OPM 2), so that $P_{pv-wind} = 0$ W, where $V_s < V_L$. As expected for this operating mode, it is noticed that portion of the active power extracted from the utility grid passes by the parallel and series inverters of the UPQC. Moreover it is noted that here is a certain flow of active energy (P_{Bdc}) to the DC bus from the utility grid via parallel inverters to recompense for the system losses with the circuit breakers of NPC inverters and passive elements. As may be seen, the parallel inverter supplies the load with sinusoidal, symmetrical regulated and voltages. In addition, the variance between output and input voltage occurs through transformers coupled in series. Finally, it can be seen that the current of grid are in-phase and sinusoidal with their corresponding voltages, that is to say that the flow of harmonic elements of the load currents in parallel inverter and not in the utility grid.

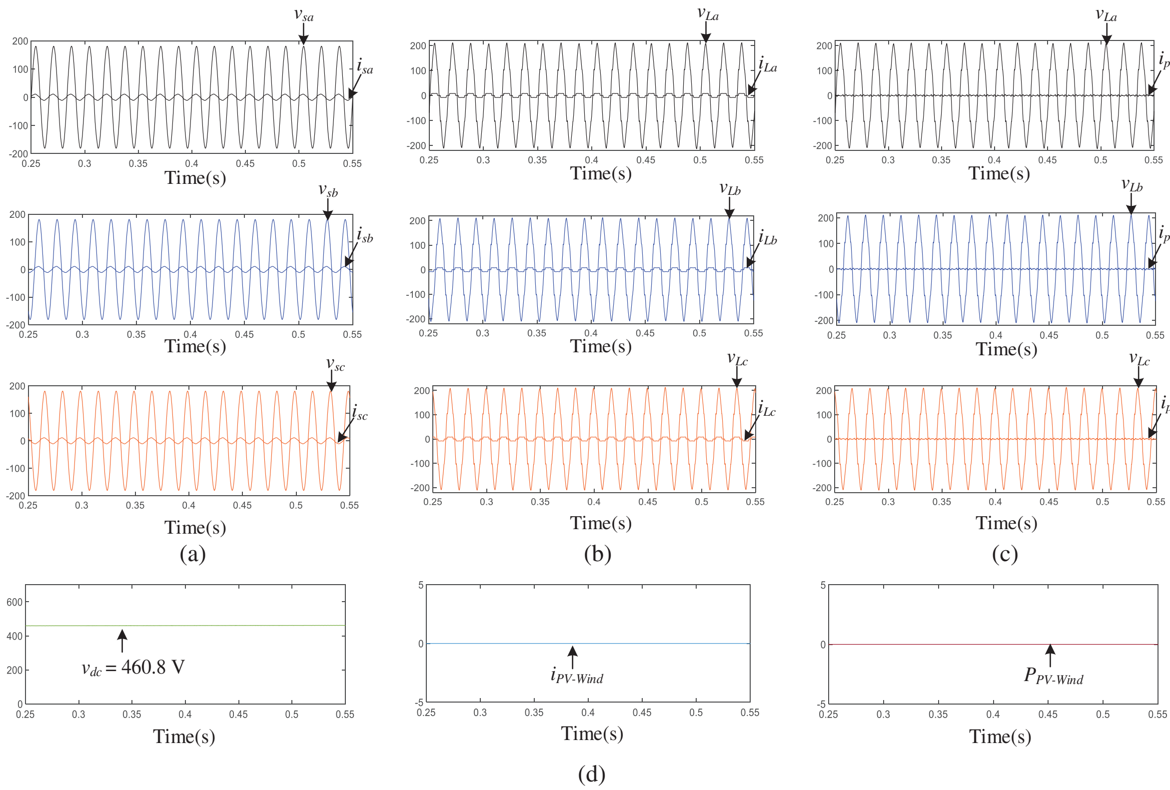

Figure 9: OPM 2: Only the active power-line conditioning is performing by PV-Wind-UPQC ($P_{pv-wind}$ = 0 W and $V_s < V_L$): (a) waveforms of the phase 'a, b and c' grid current and voltages; (b) waveforms of the phase 'a, b and c' load current and voltages; (c) waveforms of the phase 'a, b and c' parallel NPC inverter current and voltages; (d) waveforms of DC bus voltage; $i_{pv-wind}$ current; and PV array and Wind turbine Power

4.1.3 Performance of PV-Wind-UPQC at $P_{L_{abc}} = 0$ W

Fig. 10 shows the PV-Wind-UPQC system which runs without load and simply supplies the network with real power ($P_{L\_abc} = 0$ W, $V_s \cong V_L$). In this way, all the electricity produced by the system of photovoltaic and wind turbine ($P_{pv-wind}$) is fed into the utility grid, ignoring the losses of system. It may be realized that the nearly entire active power fed into the utility grid is processing by parallel converter. As may be noted, the currents of grid are in opposite phase and sinusoidal with the voltages of the grid, however the 3-Φ output voltages keeps regulated, symmetrical and sinusoidal.

Table 4 complies the measured outcomes for the system of PV-Wind-UPQC operated on OPM 1, 2 and 3. That must be noticed that entire measured values are consistent with the power flow studies described in third segment. Table 4 also illustrates the RMS values of the currents and voltages and the power factors (*PF*) and the total harmonic distortion (*THD*) associated to the load and to grid. As may be noticed, the *THDs* of the output voltages and grid currents were decreased in all types of operation and effective *PF* corrections were obtained.

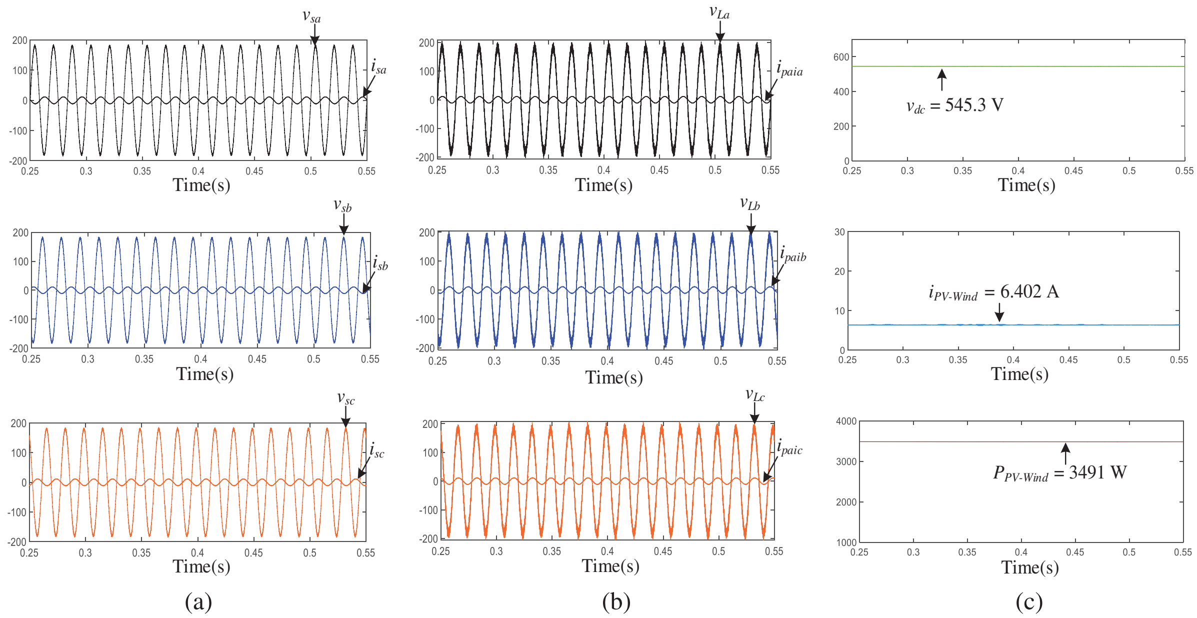

Figure 10: OPM 3: Only active power interjection is performing by PV-Wind-UPQC ($P_L = 0$ W and $V_s \cong V_L$): (a) waveforms of the phase 'a, b and c' grid currents and voltages; (b) waveforms of the phase 'a, b and c' parallel NPC inverter current and voltages; (c) waveforms of DC bus voltage; $i_{pv-wind}$ current; and PV array and Wind turbine Power

Table 4: RMS voltages and currents, *THD*, power factor and apparent and active powers

Operation modes	Phases	RMS voltages (V) and currents (A), total harmonic distortion (%) and power factor												
		Utility grid		Load		Series converter		Parallel converter		V_s/V_L	THD_{V_s}	THD_{i_l}	PF of utility grid	PF of load
		V_s	I_s	V_L	I_L	V_{sei}	I_s	V_L	I_{pai}					
OPM 1	a	127.1	2.849	128.2	6.032	10.3	2.975	128.2	8.619	0.99	1.4	29	−0.98	0.96
	b	127.1	2.836	128.2	6.017	10.37	2.982	128.2	8.586	0.99	1.4	29	−0.98	0.96
	c	127.1	2.841	128.1	6.014	9.937	2.977	128.1	8.596	0.99	1.4	29	−0.98	0.96
OPM 2	a	127.6	7.984	140.3	6.683	17.54	8.024	140.3	2.243	0.91	1.4	29	0.98	0.96
	b	127.6	7.98	139.9	6.698	17.18	7.979	139.9	2.243	0.91	1.4	29	0.98	0.96
	c	127.6	7.968	140	6.69	17.22	7.914	140	2.215	0.91	1.4	29	0.98	0.96
OPM 3	a	127.2	8.039	129.8	—	10.28	8.725	129.8	8.039	0.98	1.5	—	−0.99	—
	b	127.2	8.02	129.9	—	10.39	8.735	129.9	8.02	0.98	1.5	—	−0.99	—
	c	127.2	8.042	129.9	—	10.76	8.728	129.9	8.042	0.98	1.5	—	−0.99	—

(Continued)

Table 4 (continued)

Operation modes	Phase	Apparent (VA) and Active Powers (W)											
		Utility grid		Load		Series converter		Parallel converter		C_{Bdc}	$C_{pv\text{-}wind}$	$\frac{\lvert S_{sei}\rvert}{\lvert S_L\rvert}$	$\frac{\lvert S_{pai}\rvert}{\lvert S_L\rvert}$
		S_s	P_s	S_L	P_L	S_{sei}	P_{sei}	S_{pai}	P_{pai}				
OPM 1	a	362.1	−354.8	773.2	739.9	30.6	0.86	1105	1066	0.10	1.57	0.039	1.429
	b	360.4	−353.2	771.2	737.5	30.9	0.43	1100	1061	0.11	1.57	0.040	1.426
	c	361.1	−353.9	770.7	736.8	29.6	−0.83	1102	1062	0.11	1.57	0.038	1.429
OPM 2	a	1019	998.62	937.6	900.1	140.74	−117.79	314.7	−176.2	0.11	0	0.15	0.335
	b	1019	998.62	937.1	899.6	137.08	−113.60	313.8	−175.7	0.11	0	0.15	0.334
	c	1017	996.66	936.6	899.1	136.28	−117.16	310.1	−161.3	0.11	0	0.15	0.331
OPM 3	a	1023	−1009	—	—	89.69	−8.19	1044	1027	—	—	—	—
	b	1021	−1006	—	—	90.78	−2.82	1042	1025	—	—	—	—
	c	1023	−1008	—	—	93.94	−13.07	1044	1027	—	—	—	—

From the simulation results obtained from Figs. 8–10 and Table 4, it may be shown that the system can function in various modes of action and provides sinusoidal, symmetrical and regulated voltages to three phase loads. Furthermore, the system is able of efficient power/dissipation from/to the three-phase utility grid with high power factor.

4.2 Dynamic Results

The dynamic performance of the system of PV-Wind-UPQC has been tested taking in to account sudden changes in wind speed and solar radiation such as 100% to 0% and 0% to 100%. The dynamic consequences of wind speed changes and sudden changes in solar radiation are illustrated in Fig. 11 where the grid current (i_{sa}) and voltage (v_{sa}) across PCC 1, the voltage of load (v_{La}) across PCC 2, and power of wind and photovoltaic system ($P_{pv-wind}$) are shown. The tests were carried out by disconnecting and reconnecting the wind and photovoltaic systems from the DC bus.

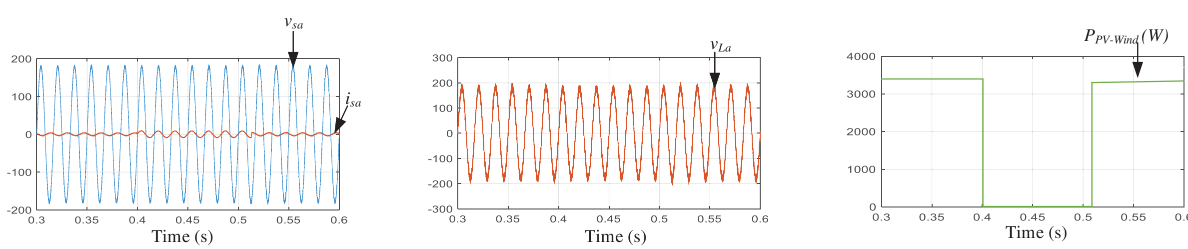

Figure 11: Active filtering along with active power interjection is performing by PV-Wind-UPQC with $P_{pv-wind} > P_L$. Phase 'a' grid current and grid voltage, load voltage, and wind and photovoltaic power $P_{pv-wind}$ for sudden wind and solar irradiance variations

As you can see, PV-Wind-UPQC performing active filtering while the wind and photovoltaic system is off. By eliminating current harmonics and compensating for load asymmetries, sinusoidal and symmetrical mains currents are obtained. Moreover, regulated and practically sinusoidal and symmetrical load voltages are attained. The PV-Wind-UPQC system then provides approximately 3500 W of real power to the load and the grid when the wind and photovoltaic system are connected.

5 Conclusion

This paper presents comprehensive studies on the analysis of power flow and PQ improvement of a system of wind PV power generation integrated with UPQC, that are fully based on the supposed double compensation scheme and various modes of functioning.

For the study of power flow, some mathematical equations and extended standardized curves of the apparent power of parallel and series inverters are presented, along with complete analyzes of the active power flowing in the system of PV-Wind-UPQC. This study turns out to be an important method for correctly sizing power converters, considering not only the effect of certain present disturbances on the voltages of grid and the non-linear properties of the load, however also the maximum power generated through the PV and wind energy system.

The system called PV-Wind-UPQC was built using two 3-level NPC inverters connected back to back. In addition to providing active energy from the system of photovoltaic and wind turbine, the system of PV-Wind-UPQC is able to improve the power quality problems. Therefore, the both steady state and dynamic performances of the system have been assessed under disturbed/distorted line voltage situations, containing harmonics, imbalances and dips.

Static performance has been tested by taking into account various operating conditions including grid voltage, load properties, and power generation from PV array and wind turbines (OPM 1-3). However, the dynamic performance has been assessed by considering the system exposed to an abrupt change in solar radiance and wind speed. All simulation outcomes show that the proposed system of PV-WIND-UPQC is appropriate for use with better performance and high Power quality.

Data Availability Statement: The data used to support the findings can be provided on demand from the corresponding author.

Funding Statement: The authors received no specific funding for this study

Conflicts of Interest: The authors declare that they have no conflicts of interest to report regarding the present study.

References

1. Benali, A., Khiat, M., Allaoui, T., Denaï, M. (2018). Power quality improvement and low voltage ride through capability in hybrid wind-PV farms grid-connected using dynamic voltage restorer. *IEEE Access, 6,* 68634–68648. DOI 10.1109/ACCESS.2018.2878493.
2. Hossain, J., Pota, H. R. (2014). *Robust control for grid voltage stability: High penetration of renewable energy*. Singapore: Springer Singapore.
3. Malinowski, M., Leon, J. I., Abu-Rub, H. (2017). Solar photovoltaic and thermal energy systems: Current technology and future trends. *Proceedings of the IEEE, 105(11),* 2132–2146. DOI 10.1109/JPROC.2017.2690343.
4. Ramachandran, S. (2020). Applying AI in power electronics for renewable energy systems. *IEEE Power Electronics Magazine, 7(3),* 66–67.
5. Zarate, J. (2015). World energy outlook 2015–Analysis-IEA. https://www.iea.org/reports/world-energy-outlook-2015.
6. Ellabban, O., Abu-Rub, H., Blaabjerg, F. (2014). Renewable energy resources: Current status, future prospects and their enabling technology. *Renewable and Sustainable Energy Reviews, 39,* 748–764. DOI 10.1016/j.rser.2014.07.113.

7. Wang, K., Liu, C., Sun, J., Zhao, K., Wang, L. et al. (2021). State of charge estimation of composite energy storage systems with supercapacitors and lithium batteries. *Complexity, 2021(1)*. DOI 10.1155/2021/8816250.
8. Liu, C., Li, Q., Wang, K. (2021). State-of-charge estimation and remaining useful life prediction of supercapacitors. *Renewable and Sustainable Energy Reviews, 150,* 111408. DOI 10.1016/j.rser.2021.111408.
9. Feng, X., Li, Q., Wang, K. (2021). Waste plastic triboelectric nanogenerators using recycled plastic bags for power generation. *ACS Applied Materials and Interfaces, 13(1),* 400–410. DOI 10.1021/acsami.0c16489.
10. Feng, X., Zhang, Y., Kang, L., Wang, L., Duan, C. et al. (2020). Integrated energy storage system based on triboelectric nanogenerator in electronic devices. *Frontiers of Chemical Science and Engineering, 15(2),* 238–250. DOI 10.1007/s11705-020-1956-3.
11. Kang, L., Du, H., Deng, J., Jing, X., Zhang, S. et al. (2021). Synthesis and catalytic performance of a new V-doped CeO_2-supported alkali-activated-steel-slag-based photocatalyst. *Journal of Wuhan University of Technology-Mater Sci. Ed, 36(2),* 209–214. DOI 10.1007/s11595-021-2396-8.
12. Ma, C., Du, H., Liu, J., Kang, L., Du, X. et al. (2021). High-temperature stability of dielectric and energy-storage properties of weakly-coupled relaxor (1-x)$BaTio_3$-xBi(Y1/3Ti1/2)O3 ceramics. *Ceramics International, 47(17),* 25029–25036. DOI 10.1016/j.ceramint.2021.05.231.
13. Ran, H., Du, H., Ma, C., Zhao, Y., Feng, D. et al. (2021). Effects of A/B-site co-doping on microstructure and dielectric thermal stability of $AgNbO_3$ ceramics. *Science of Advanced Materials, 13(5),* 741–747. DOI 10.1166/sam.2021.3943.
14. Sadiq, M. T., Yu, X., Yuan, Z., Fan, Z., Rehman, A. U. et al. (2019). Motor imagery EEG signals classification based on mode amplitude and frequency components using empirical wavelet transform. *IEEE Access, 7,* 127678–127692. DOI 10.1109/Access.6287639.
15. Nehrir, M. H., Wang, C., Strunz, K., Aki, H., Ramakumar, R. et al. (2011). A review of hybrid renewable/alternative energy systems for electric power generation: Configurations, control, and applications. *IEEE Transactions on Sustainable Energy, 2(4),* 392–403. DOI 10.1109/TSTE.2011.2157540.
16. Hua, Y., Wang, N., Zhao, K. (2021). Simultaneous unknown input and state estimation for the linear system with a rank-deficient distribution matrix. *Mathematical Problems in Engineering, 2021(12),* 1–11. DOI 10.1155/2021/6693690.
17. Liu, C., Zhang, Y., Sun, J., Cui, Z., Wang, K. (2021). Stacked bidirectional LSTM RNN to evaluate the remaining useful life of supercapacitor. *International Journal of Energy Research, 46(3),* 3034–3043. DOI 10.1002/er.7360.
18. Xu, H., Du, H., Kang, L., Cheng, Q., Feng, D. et al. (2021). Constructing straight pores and improving mechanical properties of gangue-based porous ceramics. *Journal of Renewable Materials, 9(12),* 2129–2140. DOI 10.32604/jrm.2021.016090.
19. Bacha, S., Picault, D., Burger, B., Etxeberria-Otadui, I., Martins, J. (2015). Photovoltaics in microgrids: An overview of grid integration and energy management aspects. *IEEE Industrial Electronics Magazine, 9(1),* 33–46. DOI 10.1109/MIE.2014.2366499.
20. Zhao, J., Li, F., Wang, Z., Dong, P., Xia, G. et al. (2021). Flexible PVDF nanogenerator-driven motion sensors for human body motion energy tracking and monitoring. *Journal of Materials Science: Materials in Electronics, 32(11),* 14715–14727. DOI 10.1007/s10854-021-06027-w.
21. Kjaer, S. B., Pedersen, J. K., Blaabjerg, F. (2005). A review of single-phase grid-connected inverters for photovoltaic modules. *IEEE Transactions on Industry Applications, 41(5),* 1292–1306. DOI 10.1109/TIA.2005.853371.
22. Li, W., Gu, Y., Luo, H., Cui, W., He, X. et al. (2015). Topology review and derivation methodology of single-phase transformerless photovoltaic inverters for leakage current suppression. *IEEE Transactions on Industrial Electronics, 62(7),* 4537–4551. DOI 10.1109/TIE.2015.2399278.

23. Zhang, L., Sun, K., Feng, L., Wu, H., Xing, Y. (2013). A family of neutral point clamped full-bridge topologies for transformerless photovoltaic grid-tied inverters. *IEEE Transactions on Power Electronics, 28(2),* 730–739. DOI 10.1109/TPEL.2012.2205406.
24. Neves, F. A. S., Carrasco, M., Mancilla-David, F., Azevedo, G. M. S., Santos, V. S. (2016). Unbalanced grid fault ride-through control for single-stage photovoltaic inverters. *IEEE Transactions on Power Electronics, 31(4),* 3338–3347. DOI 10.1109/TPEL.2015.2453275.
25. Xiao, H., Xie, S. (2012). Transformerless split-inductor neutral point clamped three-level PV grid-connected inverter. *IEEE Transactions on Power Electronics, 27(4),* 1799–1808. DOI 10.1109/TPEL.2011.2164940.
26. Wu, L., Zhao, Z., Liu, J. (2007). A Single-stage three-phase grid-connected photovoltaic system with modified MPPT method and reactive power compensation. *IEEE Transactions on Energy Conversion, 22(4),* 881–886. DOI 10.1109/TEC.2007.895461.
27. Cavalcanti, M. C., Farias, A. M., Oliveira, K. C., Neves, F. A. S., Afonso, J. L. (2012). Eliminating leakage currents in neutral point clamped inverters for photovoltaic systems. *IEEE Transactions on Industrial Electronics, 59(1),* 435–443. DOI 10.1109/TIE.2011.2138671.
28. Tang, Y., Yao, W., Loh, P. C., Blaabjerg, F. (2016). Highly reliable transformerless photovoltaic inverters with leakage current and pulsating power elimination. *IEEE Transactions on Industrial Electronics, 63(2),* 1016–1026. DOI 10.1109/TIE.2015.2477802.
29. Kim, Y., Cha, H., Song, B. M., Lee, K. Y. (2012). Design and control of a grid-connected three-phase 3-level NPC inverter for building integrated photovoltaic systems. *2012 IEEE PES Innovative Smart Grid Technologies*, pp. 1–7. Washington DC, USA.
30. Ding, G., Gao, F., Tian, H., Ma, C., Chen, M. et al. (2016). Adaptive DC-link voltage control of two-stage photovoltaic inverter during low voltage ride-through operation. *IEEE Transactions on Power Electronics, 31(6),* 4182–4194. DOI 10.1109/TPEL.2015.2469603.
31. da Silva, S., Ol, A., Sampaio, L. P., de Oliveira, F. M., Durand, F. R. (2017). Feed-forward DC-bus control loop applied to a single-phase grid-connected PV system operating with PSO-based MPPT technique and active power-line conditioning. *IET Renewable Power Generation, 11(1),* 183–193. DOI 10.1049/iet-rpg.2016.0120.
32. Wu, T. F., Nien, H. S., Shen, C. L., Chen, T. M. (2005). A single-phase inverter system for PV power injection and active power filtering with nonlinear inductor consideration. *IEEE Transactions on Industry Applications, 41(4),* 1075–1083. DOI 10.1109/TIA.2005.851035.
33. Sezen, S., Aktaş, A., Uçar, M., Özdemir, E. (2017). Design and operation of a multifunction photovoltaic power system with shunt active filtering using a single-stage three-phase multilevel inverter. *Turkish Journal of Electrical Engineering and Computer Sciences, 25(2),* 1412–1425. DOI 10.3906/elk-1602-381.
34. Campanhol, L. B. G., da Silva, S. A. O., de Oliveira, A. A., Bacon, V. D. (2017). Dynamic performance improvement of a grid-tied PV system using a feed-forward control loop acting on the NPC inverter currents. *IEEE Transactions on Industrial Electronics, 64(3),* 2092–2101. DOI 10.1109/TIE.2016.2625779.
35. Guerrero, J. M., Loh, P. C., Lee, T. L., Chandorkar, M. (2013). Advanced control architectures for intelligent microgrids–Part II: Power quality, energy storage, and AC/DC microgrids. *IEEE Transactions on Industrial Electronics, 60(4),* 1263–1270. DOI 10.1109/TIE.2012.2196889.
36. Rocabert, J., Luna, A., Blaabjerg, F., Rodríguez, P. (2012). Control of power converters in AC microgrids. *IEEE Transactions on Power Electronics, 27(11),* 4734–4749. DOI 10.1109/TPEL.2012.2199334.
37. IEEE Power & Energy Society (2010). *IEEE standard definitions for the measurement of electric power quantities under sinusoidal, nonsinusoidal, balanced, or unbalanced conditions*. IEEE Std. 1459–2010.
38. Teke, A., Saribulut, L., Tumay, M. (2006). A novel reference signal generation method for power-quality improvement of unified power-quality conditioner. *IEEE Transactions on Power Delivery, 26(4),* 2205–2214.
39. Devassy, S., Singh, B. (2016). Dynamic performance of solar PV integrated UPQC-P for critical loads. *2015 Annual IEEE India Conference*, pp. 1–6. New Delhi, India.

40. Han, B., Bae, B., Kim, H., Baek, S. (2006). Combined operation of unified power-quality conditioner with distributed generation. *IEEE Transactions on Power Delivery, 21(1),* 330–338. DOI 10.1109/TPWRD.2005.852843.
41. Campanhol, L. B. G., da Silva, S. A. O., de Oliveira, A. A., Bacon, V. D. (2017). Single-stage three-phase grid-tied pv system with universal filtering capability applied to DG systems and AC microgrids. *IEEE Transactions on Power Electronics, 32(12),* 9131–9142. DOI 10.1109/TPEL.2017.2659381.
42. Modesto, R. A., Oliveira da Silva, S. A., de Oliveira Júnior, A. A. (2015). Power quality improvement using a dual unified power quality conditioner/uninterruptible power supply in three-phase four-wire systems. *IET Power Electronics, 8(9),* 1595–1605. DOI 10.1049/iet-pel.2014.0734.
43. Modesto, R. A., da Silva, S. A. O., de Oliveira, A. A., Bacon, V. D. (2016). A versatile unified power quality conditioner applied to three-phase four-wire distribution systems using a dual control strategy. *IEEE Transactions on Power Electronics, 31(8),* 5503–5514. DOI 10.1109/TPEL.63.
44. França, B. W., da Silva, L. F., Aredes, M. A., Aredes, M. (2015). An improved iUPQC controller to provide additional grid-voltage regulation as a STATCOM. *IEEE Transactions on Industrial Electronics, 62(3),* 1345–1352. DOI 10.1109/TIE.2014.2345328.
45. Fujita, H., Akagi, H. (1998). The unified power quality conditioner: The integration of series- and shunt-active filters. *IEEE Transactions on Power Electronics, 13(2),* 315–322. DOI 10.1109/TPEL.63.
46. Riaz, S., Lin, H., Waqas, M., Afzal, F., Wang, K. et al. (2021). An accelerated error convergence design criterion and implementation of lebesgue-p norm ILC control topology for linear position control systems. *Mathematical Problems in Engineering, 2021(8),* 1–12. DOI 10.1155/2021/5975158.
47. Riaz, S., Lin, H., Afzal, F., Maqbool, A. (2021). Design and implementation of novel LMI-based iterative learning robust nonlinear controller. *Complexity, 2021(1),* 1–13. DOI 10.1155/2021/5577241.
48. Riaz, S., Lin, H., Akhter, M. P. (2020). Design and implementation of an accelerated error convergence criterion for norm optimal iterative learning controller. *Electronics, 9(11),* 1766. DOI 10.3390/electronics9111766.
49. Riaz, S., Lin, H., Elahi, H. (2021). A novel fast error convergence approach for an optimal iterative learning controller. *Integrated Ferroelectrics, 213(1),* 103–115. DOI 10.1080/10584587.2020.1859828.
50. Riaz, S., Lin, H., Mahsud, M., Afzal, D., Alsinai, A. et al. (2021). An improved fast error convergence topology for PD α-type fractional-order ILC. *Journal of Interdisciplinary Mathematics, 24(7),* 2005–2019. DOI 10.1080/09720502.2021.1984567.
51. Riaz, S., Lin, H., Anwar, M. B., Ali, H. (2020). Design of PD-type second-order ILC law for PMSM servo position control. *Journal of Physics Conference Series, 1707(1),* 012002. DOI 10.1088/1742-6596/1707/1/012002.
52. Bouzelata, Y., Kurt, E., Chenni, R., Altin, N. (2015). Design and simulation of a unified power quality conditioner fed by solar energy. *International Journal of Hydrogen Energy, 40(44),* 15267–15277. DOI 10.1016/j.ijhydene.2015.02.077.
53. Srikanth, K. S., Mohan, T. K., Vishnuvardhan, P. (2015). Improvement of power quality for microgrid using fuzzy based UPQC controller. *2015 International Conference of Electrical, Electronics, Signals, Commuication and Optimization*, pp. 1–6. Visakhapatnam, India.
54. Toodeji, H., Fathi, S. H., Gharehpetian, G. B. (2009). Power management and performance improvement in integrated system of variable speed wind turbine and UPQC. *2009 International Conference on Clean Electical. Power*, pp. 609–614. Capri, Italy.
55. Hosseinpour, M., Yazdian, A., Mohamadian, M., Kazempour, J. (2008). Design and simulation of UPQC to improve power quality and transfer wind energy to grid. *Journal of Applied Sciences, 8(21),* 3770–3782. DOI 10.3923/jas.2008.3770.3782.
56. Bhavani, R., Prabha, N. R., Kanmani, C. (2015). Fuzzy controlled UPQC for power quality enhancement in a DFIG based grid connected wind power system. *IEEE 2015 International Conference on Circuits, Power and Computing Technologies*, Nagercoil, India.

57. Díaz, N. L., Vasquez, J. C., Guerrero, J. M. (2018). A Communication-less distributed control architecture for islanded microgrids with renewable generation and storage. *IEEE Transactions on Power Electronics, 33(3),* 1922–1939. DOI 10.1109/TPEL.2017.2698023.
58. Campanhol, L. B. G., da Silva, S. A. O., de Oliveira, A. A., Bacon, V. D. (2109). Power flow and stability analyses of a multifunctional distributed generation system integrating a photovoltaic system with unified power quality conditioner. *IEEE Transactions on Power Electronics, 34(7),* 6241–6256. DOI 10.1109/TPEL.63.
59. Reisi, A. R., Moradi, M. H., Showkati, H. (2013). Combined photovoltaic and unified power quality controller to improve power quality. *Solar Energy, 88,* 154–162. DOI 10.1016/j.solener.2012.11.024.
60. Al-Quraan, A., Al-Qaisi, M. (2021). Modelling, design and control of a standalone hybrid PV-wind micro-grid system. *Energies, 14(16),* 4849. DOI 10.3390/en14164849.
61. Tan, K. T., So, P. L., Chu, Y. C., Chen, M. Z. Q. (2013). A flexible AC distribution system device for a microgrid. *IEEE Transactions on Energy Conversion, 28(3),* 601–610.
62. Amirullah, A., Penangsang, O., Soeprijanto, A. (2019). Matlab/simulink simulation of unified power quality conditioner-battery energy storage system supplied by PV-wind hybrid using fuzzy logic controller. *International Journal of Electrical and Computer Engineering, 9(3),* 1479–1945. DOI 10.11591/ijece.v9i3.pp1479-1495.
63. Bacon, V. D., da Silva, S. A. O. (2015). Performance improvement of a three-phase phase-locked-loop algorithm under utility voltage disturbances using non-autonomous adaptive filters. *IET Power Electronics, 8(11),* 2237–2250. DOI 10.1049/iet-pel.2014.0808.
64. Colak, I., Kabalci, E., Bayindir, R. (2011). Review of multilevel voltage source inverter topologies and control schemes. *Energy Conversion and Managment, 52(2),* 1114–1128. DOI 10.1016/j.enconman.2010.09.006.

Appendix

SIMULATION PARAMETERS: Utility grid voltage: 127.27 V(L-N), 60 Hz; Voltage of Dc link: 616 V; Capacitance of Dc link: 4700 µF; Parallel Converter interfacing inductor: 1.73 mH; Parallel Converter interfacing inductor: 60 µF, series converter interfacing inductor: 1.75 mH; Internal resistances of parallel and series NPC converter inductors = 0.2 Ω; $P_{pv-wind} = 3.5$ kW; Minimum DC bus voltage = 460; NPC inverters switching frequency = 20 kHz; P&O-based MPPT step size voltage $(\Delta v) = 1$ V; PWM gain = 0.0002; Three phase full bridge rectifier followed via Resistive load, R = 40 Ω (S_{La} = 773.2 VA, S_{Lb} = 771.2 VA, S_{Lc} = 770.7 VA, P_{La} = 739.9 W, P_{Lb} = 737.5 W, P_{Lc} = 736.8 W).